View metadata, citation and similar papers at core.ac.uk

brought to you by CORE

provided by Via Sapientiae: The Institutional Repository at DePaul University

DePaul University

Via Sapientiae

College of Science and Health Theses and Dissertations

College of Science and Health

Winter 3-19-2016

Chemical Reaction Kinetics of the Pictet-Spengler Reaction

Jo Ann K. Girel
DePaul University, jkbialo@yahoo.com

Follow this and additional works at: https://via.library.depaul.edu/csh_etd

 Part of the Chemistry Commons

Recommended Citation

Girel, Jo Ann K., "Chemical Reaction Kinetics of the Pictet-Spengler Reaction" (2016). *College of Science and Health Theses and Dissertations*. 142.
https://via.library.depaul.edu/csh_etd/142

This Thesis is brought to you for free and open access by the College of Science and Health at Via Sapientiae. It has been accepted for inclusion in College of Science and Health Theses and Dissertations by an authorized administrator of Via Sapientiae. For more information, please contact digitalservices@depaul.edu.

Chemical Reaction Kinetics of the Pictet-Spengler Reaction

A Thesis

Presented in

Partial Fulfillment of the

Requirements for the Degree of

Master of Science

January, 2016

BY

Jo Ann Kathy Girel

Department of Chemistry

College of Science and Health

DePaul University

Chicago, Illinois

For my mom, I wouldn’t have been able to do this without you. You formed me through your example, taught me how to be strong, especially in the hardest moments of life, faithful, loving, and of course, to reach for the stars.

Table of Contents

Chapter 1 5

Tetrahydroisoquinoline Alkaloids in Medicinal Chemistry 5

The Pictet-Spengler Reaction 6

Proposed Reaction Mechanisms 8

Chapter 2 – Finding a Buffer to Compare to Phosphate and Identification of a Reaction Side Product 11

2.1 Introduction 11

2.2 Methods 12

Pictet-Spengler Reactions Monitored by HPLC-UV 12

2.3 Results 13

Side Product Identification 13

Buffer Comparison 15

Conclusion 17

Chapter 3 – Determination of Area Extinction Coefficients 18

3.1 Introduction 18

3.2 Methods 18

Standard solutions 19

Measurement of THI and isoTHI area extinction coefficients, Method A 19

Simultaneous measurement of THI and isoTHI area extinction coefficient, Method B 20

3.3 Results and Discussion 20

Method A 21

Method B 21

Conclusion 22

Chapter 4 - HPLC kinetics and Analysis of Time Course Data 23

4.1 Introduction 23

Catalysis in the Pictet-Spengler Reaction 23

The Curtin-Hammett Principle 26

4.2 Methods 27

4.3 Results 28

General Base Catalysis 29

Curtin-Hammett Principle 30

Acid/Base Catalysis 32
General Acid/ Base Catalysis Rate Constants 34
Conclusions 35
Chapter 5 – Maleic Acid Buffer and Kinetic Isotope Effects 36
5.1 Introduction 36
5.2 Methods 37
Preparation of Maleic Acid Buffer 37
High Resolution Mass Spectrometry 37
5.3 Results 37
High Resolution Mass Spectrometry 37
General Catalysis in Maleic Acid 39
Curtin-Hammett Principle Application 40
Kinetic Isotope Effects 41
Kinetic Isotope Effects in Other Studies 47
Chapter 6 – Conclusions and Future Work 50
Future Directions 51
References 52

Chapter 1

Tetrahydroisoquinoline Alkaloids in Medicinal Chemistry

Alkaloids, low-molecular weight compounds that commonly contain basic nitrogen, are produced by plants, bacteria, fungi, and animals. Alkaloid producing plants have been used for ages for vast therapeutic applications including in teas, medicines, poisons and tinctures for at least 4,000 years. The knowledge of medicinal and toxic properties of plants has been beneficial and valued to civilizations ranging from Assyria to China. In Assyria, 4,000-year-old plates have been found mentioning and describing 250 different plants. In India, details of the traditional medicine are documented in the Ayurveda. The knowledge of these alkaloid-producing plants reached the Mediterranean where medicinal plants were documented on the Ebers papyrus. Ancient Greeks and Romans, including Hippocrates and Aristotle, also utilized this knowledge, describing hundreds of medicinal plants. In the early 19th century, modern techniques were applied to isolate alkaloids. Opium, which is used as an analgesic and narcotic, was first researched leading to the isolation of morphine. In 1939, hundreds of alkaloids, including strychnine, emetine, brucine, caffeine, piperine, quinine, cinchonine and colchinine, were discovered and isolated. Today, most of the pharmaceutical drugs commonly used come from natural sources and serve as models in discovering effective drugs. [1]

Pharmaceutical alkaloids have various applications including the ability to affect the nervous system (GABA, dopamine, and serotonin), have antihypertensive effects (indole alkaloids), antimalarial activity (quinine), anticancer effects (dimeric indoles), antibiotic effects (berberine), analgesics (morphine), antitussive (codeine), etc. Over the last 50 years, an estimated 53 alkaloids are currently being used for pharmaceutical applications.[2]Due to the importance of these natural products in medicinal chemistry, the development of novel pharmaceutical alkaloids is imperative not only to discover new applications but also to serve as a scaffold for novel compounds and as starting materials for semisynthetic compounds.

The Pictet-Spengler reaction of dopamine with 4-hydroxyphenyl-acetaldehyde (4-HPAA) (Figure 1) is the first step in the biosynthesis thousands of known alkaloids. This diversity of final products is generated by further tailoring reactions. Naturally inspired drug candidates can be made the same way, with enzymes from natural biosynthetic pathways or by chemical reactions. The Pictet-Spengler reaction of the substrates in question is particularly relevant because the chemical reaction generates a racemic mixture of norcoclaurine but enzymes only generate (S)-norcoclaurine. Because phosphate is so specific for catalysis, it is a perfect candidate for investigation of a chiral catalyst that can possibly control the stereoselectivity. Understanding the specificity of phosphate may help chemists design such catalysts.[3]

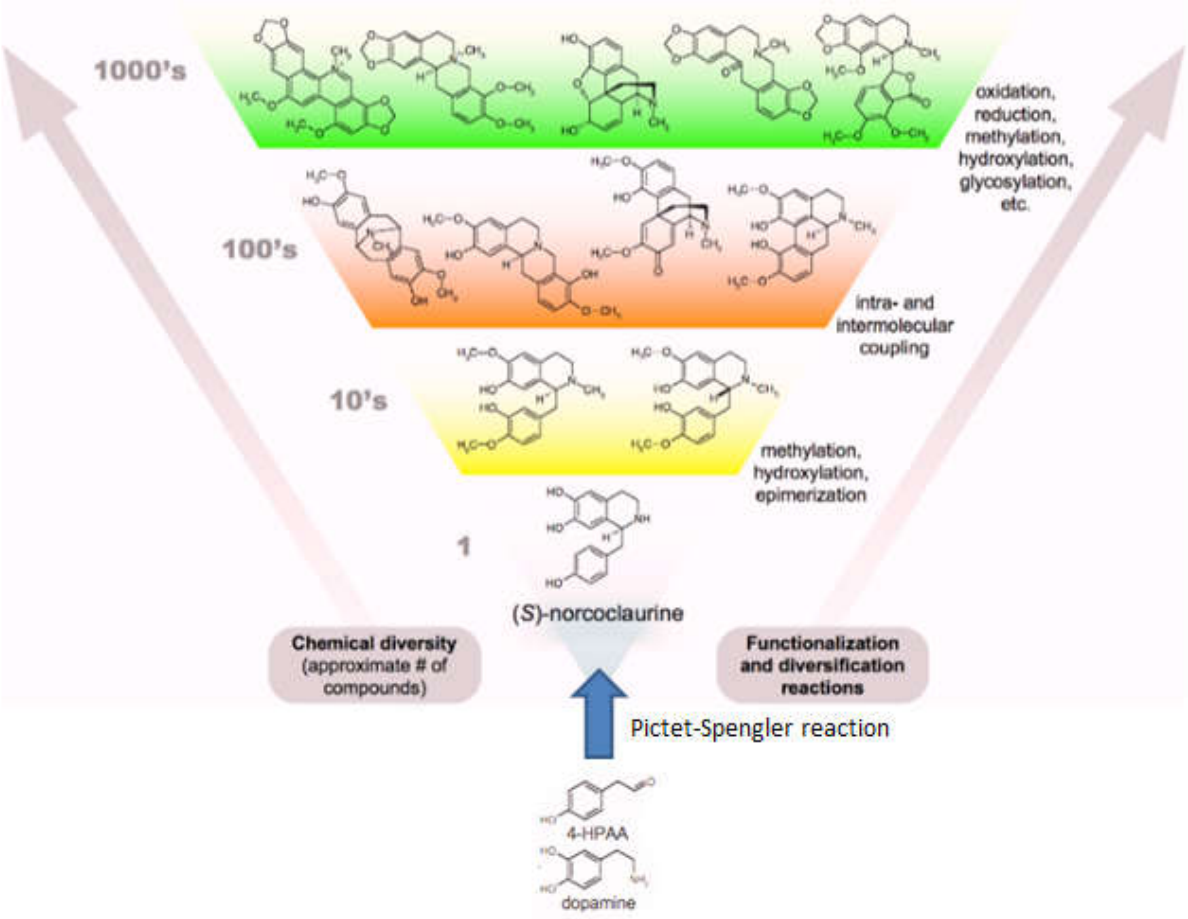

Figure 1. Vast chemical diversity of natural products beginning from the Pictet-Spengler reaction of dopamine and 4-HPAA to form (S)-norcoclaurine Adapted from Libsombe,2008 .[4]

The Pictet-Spengler Reaction

The Pictet-Spengler reaction is a two-step chemical cyclization reaction which was discovered by Amé Pictet and Theodor Spengler in 1911 by heating β-phenylethylamine and formaldehyde dimethylacetal in the presence of hydrochloric acid. The reaction they described formed the alkaloid 1,2,3,4-tetrahydroisoquinoline (THI). The mechanism (Scheme 1) begins with the protonation of the carbonyl oxygen (**1**) by the acid which is attacked by the amine reagent. An iminium intermediate (**2**) is formed through proton transfer steps and the release of a water molecule which then undergoes 6-endo-trig cyclization reaction, resulting in the loss of aromaticity of the aryl ring. The final deprotonation step restores the aromaticity and results in the product THI (**3**).[5 5 6]

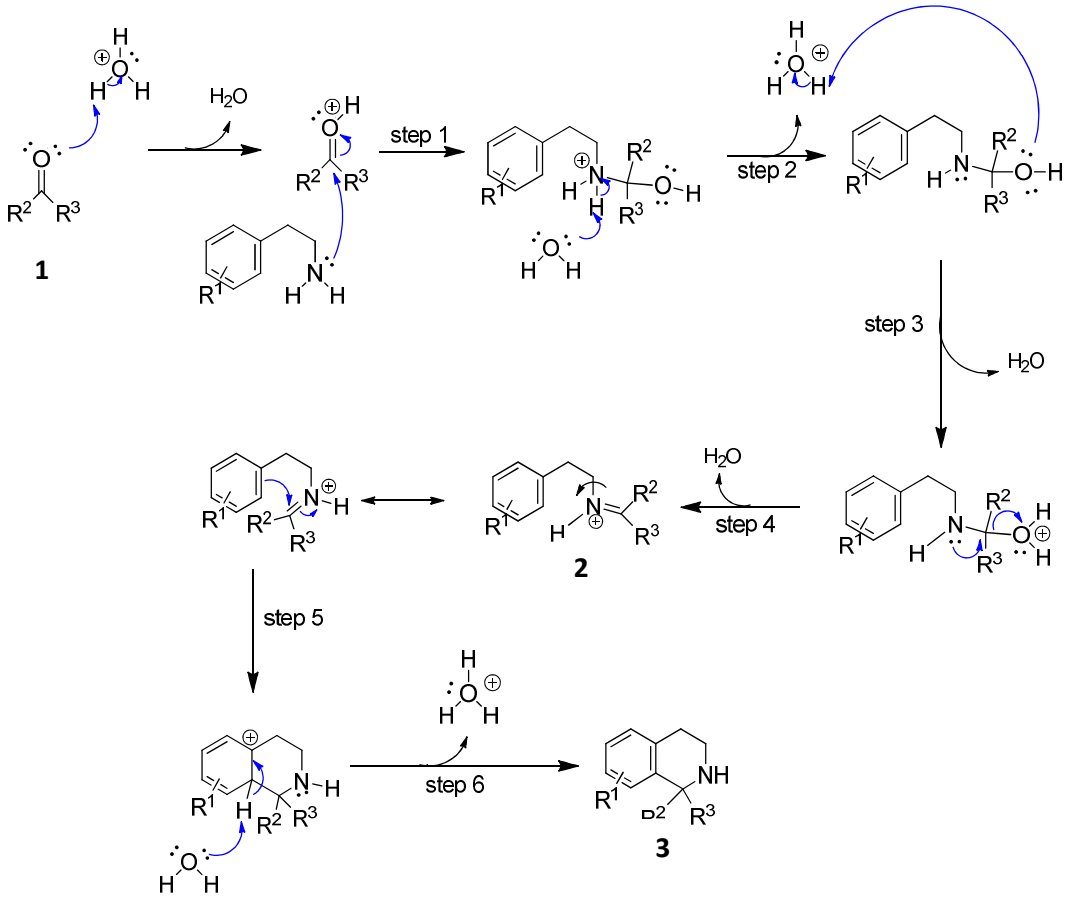

Scheme 1. Mechanism of the Pictet-Spengler reaction where a β-arylenylamine and an aldehyde convert to form a tetrahydroisoquinoline using an acid catalyst.

This mechanism has been studied extensively with most of the previous work focused on Pictet-Spengler condensations with highly reactive indoles, such as tryptamine. [5] The Pictet-Spengler condensation reaction between tryptamine and an aldehyde occurs in very mild conditions. Cook et al. reviewed the data for the reaction of benzaldehyde and tryptamine being prepared at room temperature in a nonacidic, aprotic media. Under these conditions, the yield was found to be higher than in aqueous, acidic media. [5] A linear relationship between the rate and acidity of the medium was found, indicating that there is additional protonation of the *N*-monoprotonated imines (**3**) forming superelectrophiles (**4**). Pictet-Spengler reactions with phenethylamines generally require superacids to increase the electrophilicity of the iminium by generating a carbocation(Scheme 2).[7] This chemistry is utilized for synthetic applications; however this linear relationship observed between the rate and acidity of the medium adds valuable insight on the Pictet-Spengler mechanism.

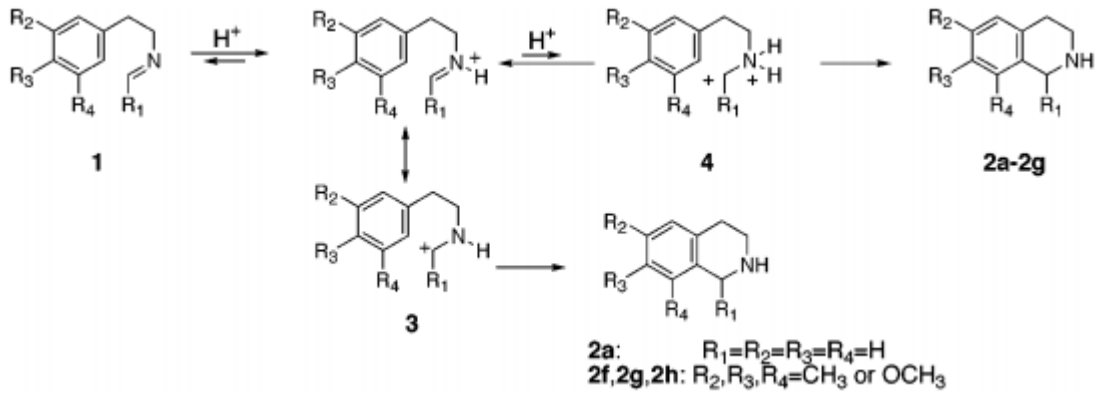

*Scheme 2. Superacid-catalyzed Pictet-Spengler reactions of imines (**1**) of 2-phenyethylamine to give the parent (**2a-2g**) and 1-substituted 1,2,3,4-tetrahydroisoquinoline in moderate to high yields.*[7]

In contrast to the indole reaction, the Pictet-Spengler reaction between 4-hydroxyphenethylamine (4-HPAA) compounds such as dopamine and aldehydes, occur readily under mild conditions (**Error! Reference source not found.**Scheme 3).[3c] The reaction is initiated by formation of a carbinolamine (aminol), followed by elimination of water to form an iminium cation. The subsequent rate-limiting step, deprotonation of the dopamine 3-hydroxy, triggers cyclization onto the iminium. The final deprotonation step forms the THI (e.g. norcoclaurine for R = C_5H_4OH). The formation of (S)-norcoclaurine is greatly studied because this compound is the starting compound in benzylisoquinoline alkaloid (BIA) biosynthesis. (Figure 1). [8]

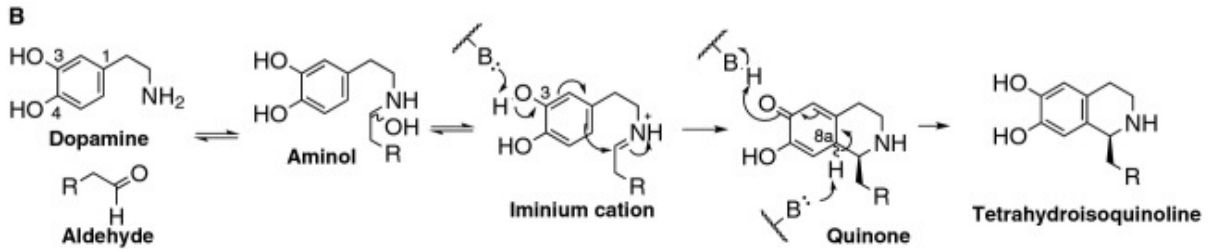

Scheme 3. Pictet-Spengler reaction of dopamine and aldehyde to form tetrahydroisoquinoline . [3c]

Proposed Reaction Mechanisms

The reaction was further studied by Pesnot et. al who demonstrated that near neutral pH, the conversion rate of the Pictet-Spengler reaction between equimolar 4-HPAA and dopamine increased to 77% by increasing the temperature reaction to 50°C. In addition, Pesnot et al. noted that at pH 6.0, phosphate catalyzes the reaction much more effectively than other buffers.[3c] (Chapter 2, Table 1). Buffers that do not contain phosphate have very low conversion rates whereas phosphate-containing buffers have effective catalytic activity. Interestingly, diphosphate (pyrophosphate) has half the rate of phosphate-containing buffers.

Pesnot et al. proposed two possible mechanisms to explain the apparent specificity of phosphate catalysis (see Scheme 4). In *path a* of Scheme 4, phosphate ion forms a phosphate carbinolamine and the resulting a 6-exo-tet ring closure is facilitated by the phosphate leaving group. The role of phosphate is to act as a nucleophile by formation of an unusual phosphate carbinolamine that is apparently more electrophilic than the iminium. By *path b*, the role of phosphate is to deprotonate to make the aromatic ring more nucleophilic for 6-endo-trig substitution. In this mechanism, phosphate is a base catalyst. Neither of these mechanisms explains the apparent uniqueness of phosphate ion in the reaction mechanism.

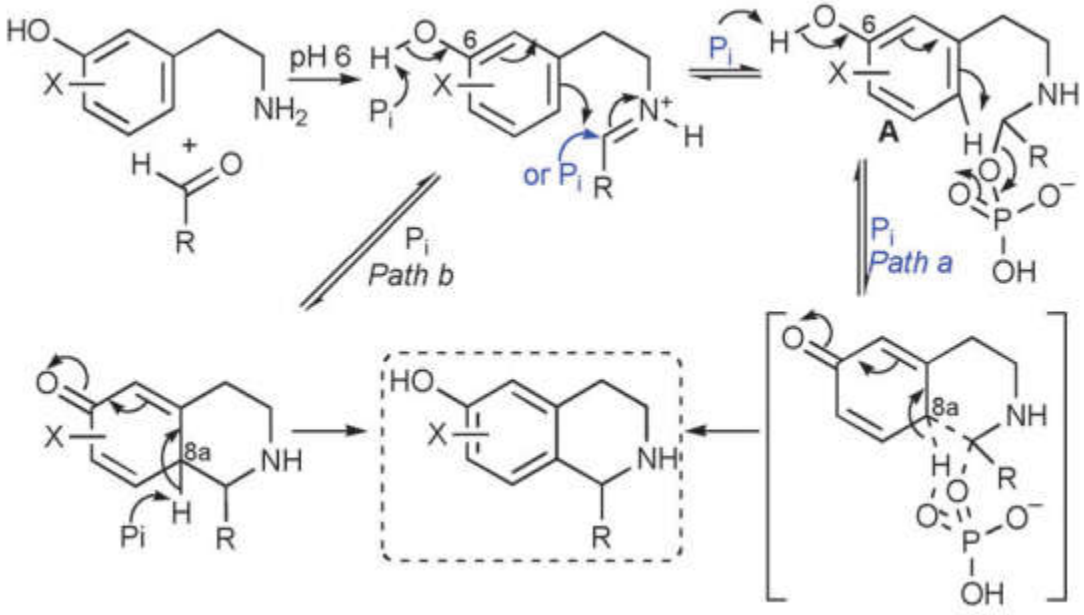

Scheme 4. Possible reaction mechanism for phosphate catalysis proposed by Pesnot el al.[3c]

The mechanism of the Pictet-Spengler reaction will be studied to determine if the phosphate ion is a selective catalyst for the reaction and whether the ability to selectively catalyze other reactions or generate phosphate-based catalysts that control the stereoselectivity in this reaction.

In collaboration with Dr. Ruben Parra, we have found no theoretical evidence for *path a*. We have examined possible energy landscapes for *path b* as well as alternative mechanisms involving phosphate. For example, by one alternative proposal by Dr. Ruben Parra, phosphate catalyzes the Pictet-Spengler condensation through the involvement of two phosphate ions forming a hydrogen bond network (Scheme 5). Although, this mechanism requires the infrequent situation of three molecules to form a reactive complex, it does uniquely require the geometry of phosphate. Initial computational results also suggest that phosphate ion may selectively catalyze steps 5 and 6 in Scheme 1 as a single transition state.[9]

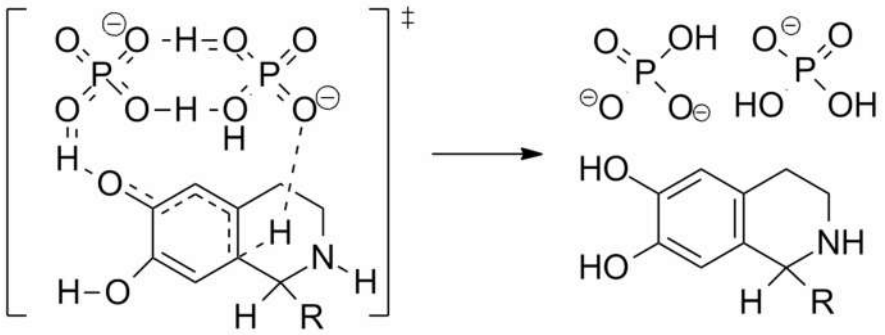

Scheme 5. Proposed transition state in which two phosphate ions form a hydrogen bond network.

In principle, any of these proposals can be supported or eliminated with experimental evidence. In this thesis, an experimental investigation of the mechanism of the Pictet-Spengler reaction through kinetic studies in phosphate buffer will be presented and the results will be compared to those in an alternative catalytic buffer, maleic acid.

For all studies, the reaction of dopamine and propanal were examined as a model system. The most common substrate for this reaction in biology, 4-HPAA, was not selected because is not soluble in water above 10 mM. [10] Furthermore, the compound is not commercially available and needs to be prepared.[10] Moreover, 4-HPAA has an additional reactive phenol group that could potentially complicate mechanistic interpretations. Propanal is the lowest molecular weight aldehyde that is liquid at room temperature. Given that it is readily available and has no other potentially catalytic reactive groups, it was selected as the aldehyde for all experiments. Propanal has the additional benefit of being small enough to model computationally.

Chapter 2 – Finding a Buffer to Compare to Phosphate and Identification of a Reaction Side Product

2.1 Introduction

Pesnot et al. cataloged the relative reaction rate of the Pictet-Spengler reaction of dopamine and 4-HPAA in several buffers. Many of these buffers did not have pKa values that were similar to phosphate (Table 1). Pesnot et al. found that the buffers with potassium or sodium salts of phosphate, UMP and Glc-1-P have high conversion rates for the Pictet-Spengler reaction of phenylacetaldehyde with various phenethethylamines. Borate and vanadate, which are known to mimic phosphate, did not catalyze the formation of products. This suggested that that there is some sort of phosphate specificity in the reaction.

Table 1. Buffer influence on Pictet-Spengler reaction of dopamine and 4-HPAA. Conversion rates given by Pesnot et. al. Reaction conditions: 4 mM dopamine, 4.8 mM 4-HPAA, and 0.1 M buffer, pH 6, 50 °C, 1 hour.

Buffer	pKa	Conversion (%)
Tris	8.3[11]	<1
HEPES	7.55[11]	<1
$B(OH)_3$	9.23[12]	<1
Na_3VO_4	3.5 8.1 12[13]	<1
$KHCO_3$	6.37 10.25[14]	2
$KHSO_4$	1.92 [15]	4
KH_2PO_4	2.15 6.82 12.38[16]	77
NaH_2PO_4	2.15 6.82 12.38[17]	75
UMP	9.5 6.4[18]	75
Glc-1-P	1.10 6.13[19]	74
$Na_4P_2O_7$	0.9, 2.0, 6.6, 9.4 [20]	45
Water	15.7	<1

It should be noted that these reactions were performed at a pH of 6.0 and at 50 °C. Interestingly, many of these compounds do not actually buffer at pH 6.0, which raises the question of whether it is actually

valid to compare them to phosphate. For example, it is possible that the catalytic fitness of a buffer was simply correlated to the solution concentration of conjugate acid and base species. The published pKa values of the buffers used by Pesnot et al. were investigated to see if this was the case, since buffer pKa influences the ratio of acid and basic catalytic species in a buffer (Table 1). There was no clear correlation between the dominant catalytic species at pH 6.0 and catalysis. Tris, borate, and ortho-vanadate were all poor catalysts and mostly protonated under the pH 6.0 reaction conditions. However, carbonate and the phosphates have similar pKa values but exhibited very different reactivity.

To identify the importance of phosphate in the Pictet-Spengler mechanism, another buffer with a pKa that is similar to monobasic phosphate (7.21) but with slower kinetics to use as a control in mechanistic experiments will need to be examined.

2.2 Methods

Pictet-Spengler Reactions Monitored by HPLC-UV

In a HPLC vial, 1.230 mL of the appropriate buffer sample (10, 20, 40, or 80 mM), 6.5 µL of 0.5 mM dopamine, and 65 µL of 100 mM propanal were mixed together. The start time was recorded as the time of addition of propanal.

Reactions were monitored using high pressure liquid chromatography on a Waters Acquity Ultra Performance Liquid Chromatography instrument with a photodiode array detector (HPLC-UV). The volume of each injection was 5 µL. The solvent and gradient conditions used for HPLC analysis were as follows: Acquity HPLC BEH C18 column (1.7 µm, 2.1x50 mm) at 25 °C; 0.4 mL/min; 0% acetonitrile (MeCN) in 0.1% aqueous trifluoroacetic acid (TFA) for 1.0 minute, 0-20% MeCN in 0.1 % TFA over 4.25 minutes, 20-70% MeCN in 0.1% TFA over 1.0 minute, hold at 70% MeCN in 0.1% TFA for 1.0 minute. Data in Figure 2 were acquired with an unoptimized method that used the same instrument and column as above but with a gradient program of 0-70% MeCN in 0.1% aqueous TFA over 5 minutes.

The time of each injection, as recorded by the computer, was documented and referenced relative to the reaction start time. Chromatograms integrated at 225 nm were analyzed and the area was recorded at the various retention times corresponding to dopamine, THI, and isoTHI (see Figure 2). At the 225 nm wavelength, the aldehyde peak is less intense than at 280 nm; therefore, when analyzing data, the ratio of aldehyde peak to product peaks does not disrupt the ability to measure the product peaks; especially for isoTHI which, in comparison, has a smaller peak.

2.3 Results

Side Product Identification

shows an HPLC trace of a typical reaction of dopamine **1** and propanal (not visible) in phosphate buffer where two products are observed. Peak **2** is the expected tetrahydroisoquinoline product (THI).

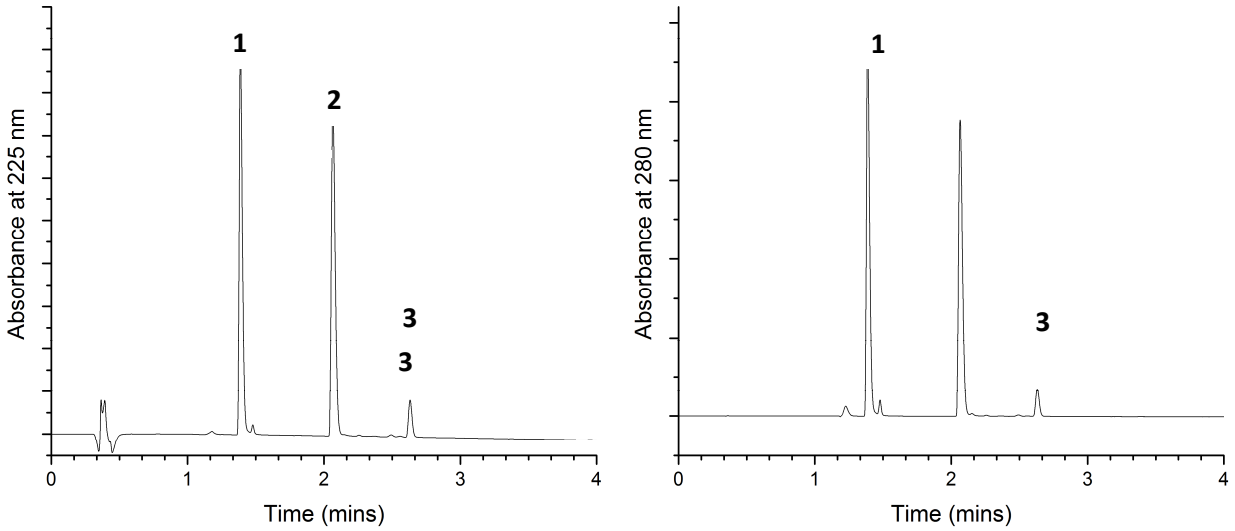

*Figure 2. HPLC chromatogram of the Pictet-Spengler reaction in phosphate buffer at 23 °C, at an absorbance of 225 nm and 280 nm, where **1** is the dopamine peak **2** is the THI peak, and **3** is the isoTHI peak.*

We suggest that Peak 3 is an isomer of tetrahydroisoquinoline, which we call isoTHI (see Scheme 6). To verify that the observed side product was not an anomaly, all solutions were remade and experiments were re-run to show if there were similar results. Further analysis continued to show similar results,

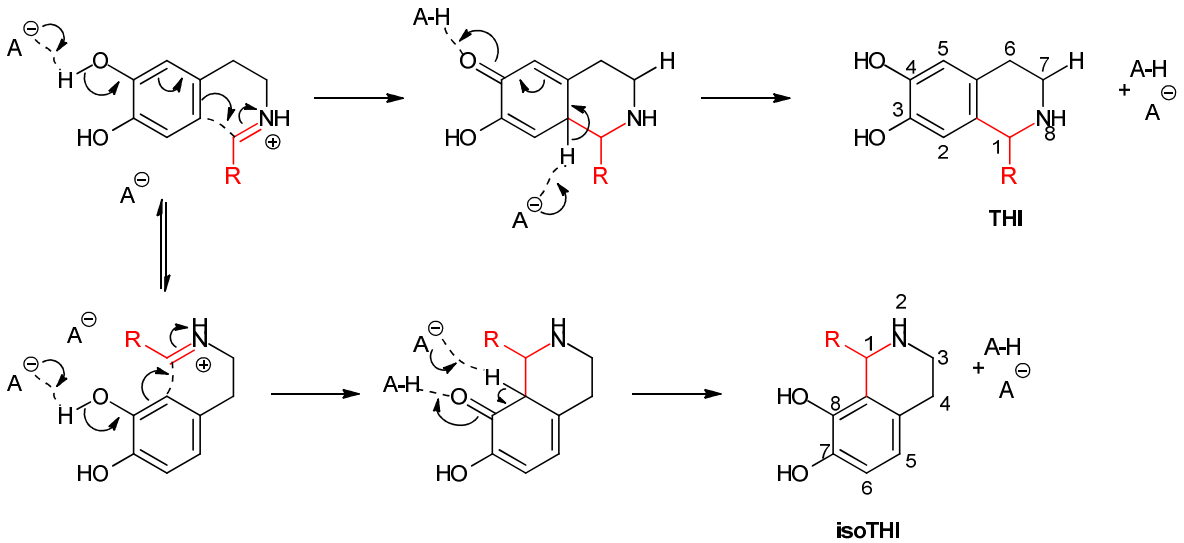

Scheme 6. Formation of tetrahydroisoquinoline (THI) and iso-tetrahydroisoquinoline (isoTHI).

which led to the suggestion that the side product was an isomer of THI (Scheme 6). This side product peak was observed in every time point for each run, increasing as the reaction continues. We were unfortunately not able to isolate or purify isoTHI. However, mass spectrophotometry was performed on THI (Figure 3) and isoTHI (Figure 4) products of the norcoclaurine synthesis and show that the spectra are identical and fragment in the same way. Therefore the best assignment with the data available suggests that THI and isoTHI are regioisomers.

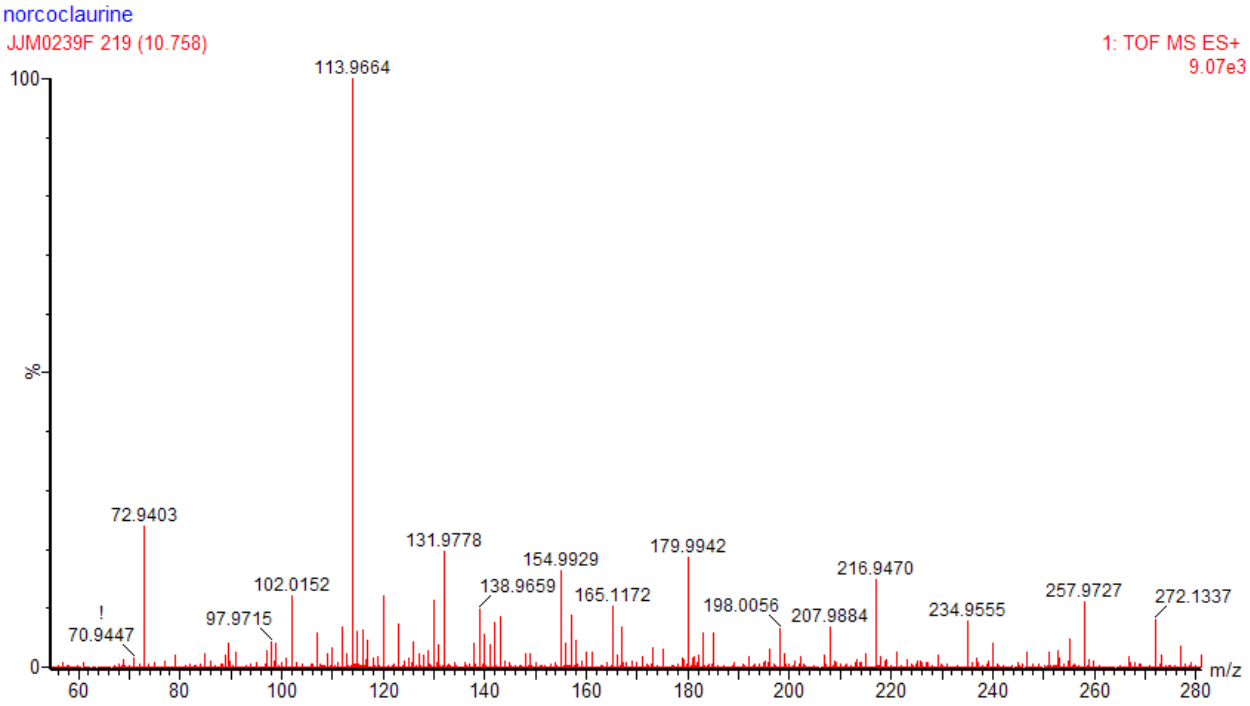

Figure 3. . High resolution mass spectrometry analysis of THI. THI is identified as m/z=272.1 showing fragments m/z= 258.0, 235.0 ,216.9,208.0,198.0,180.0,165.155.0,139.0,132.0,114.0,102.0,98.0,73.9, and 71.0.

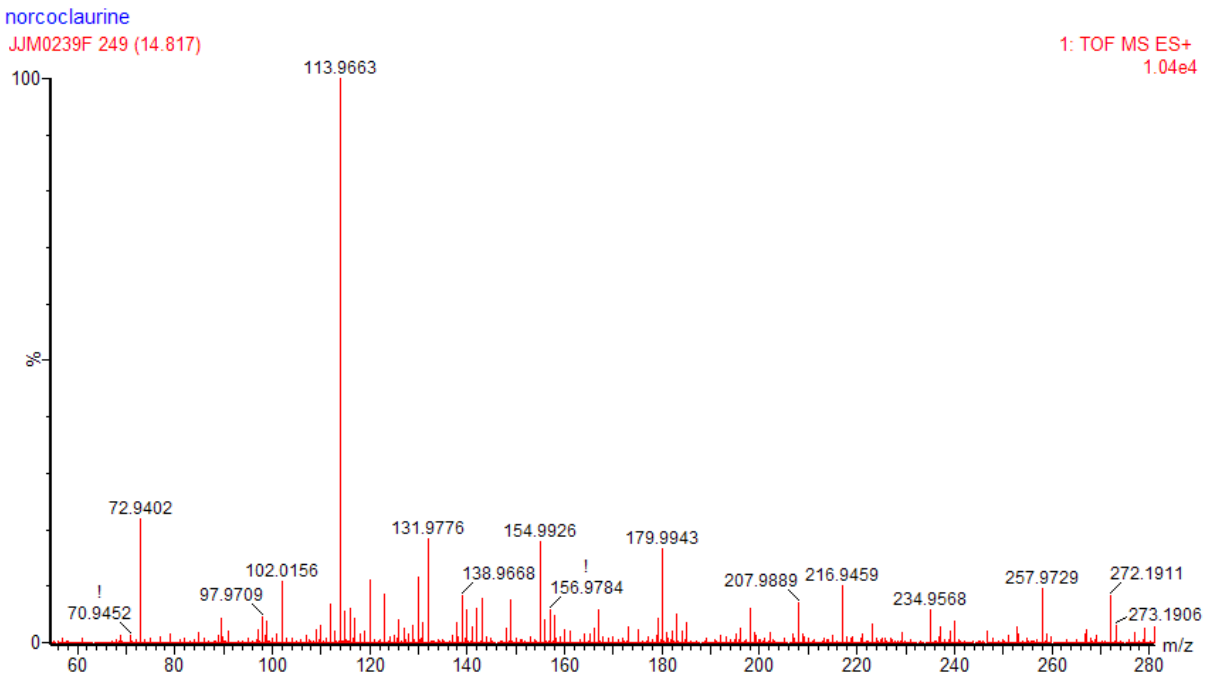

Figure 4. High resolution mass spectrometry analysis of isoTHI. isoTHI is identified as m/z=272.2 showing fragments m/z=258.0, 235.0 ,216.9,208.0,198.0,180.0,165.0,155.0,139.0,132.0,114.0,102.0,98.0,73.9, and 71.0.

Pesnot et. al do not mention or report any side product. Our lab has also observed this side product in reactions of dopamine with 4-HPAA, the same reaction studied by Pesnot et al.[10] The proposed regioisomeric side product for this reaction has been previously acknowledged in studies focused on the regioselectivity of the Pictet-Spengler reaction[21]. Quevedo et *al*. studied the Pictet-Spengler reaction with dopamine hydrobromide and different aldehydes. Isoquinonline hydrobromide was obtained in all of the reactions in high yields and complete regioselectivity. The reaction occurred in polar solvents with the starting phenylethyemine's aromatic ring having a substituent in position 1 thereby activating the ring. When two strongly activated positions were present on the dopamine ring, two isoquinoline regioisomers were formed suggesting that the activating group in position 1 of the aromatic ring is necessary for the reaction to occur. [31] If there is a side product being formed in our reaction, this raised the question of what conditions would minimize its formation. This side-product will be examined further in Chapter 3. Using the results in Figure 2 as a reference, other buffers were studied.

Buffer Comparison

Four buffers were evaluated for comparison to phosphate: imidazole (pKa=7.05) , HEPES (pKa=7.55), BES (pKa=7.15), and maleic acid (pKa=5.82).[7] The Pictet-Spengler reaction in imidazole (Figure 5), HEPES, and BES, are so slow that kinetic measurements were not practical. At high buffer concentration, the reactions required so many hours to complete that side reactions, such as the decomposition of

dopamine, through auto-oxidation of the catechol group by atmospheric oxygen and aldehyde polymerization, occurred (Figure 5). The HPLC trace of the Pictet-Spengler reaction in imidazole buffer showed no product had formed after several minutes. The reaction rate in maleic acid buffer was found to be at least 10 times faster than imidazole and slower (2 minutes) than phosphate buffer which allowed us to monitor the reaction in greater detail. To study the nature of phosphate's catalytic specificity, maleic acid was used as a comparison since the rate was fast enough that dopamine decomposition was minimal (Figure 6).

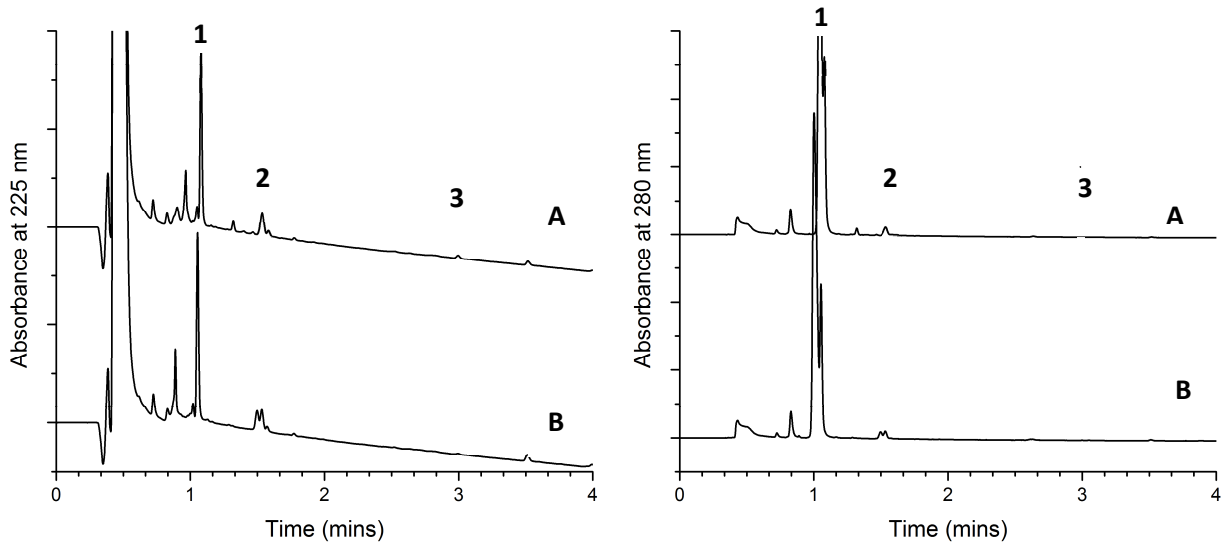

Figure 5. HPLC chromatogram of the Pictet-Spengler reaction in 40 mM imidazole buffer at an absorbance of 225 nm and 280 nm. ***A*** *represents 2 minutes into the reaction, where* ***1*** *is the imidazole peak,* ***2*** *is where the dopamine peak appears and* ***3*** *is where product THI appears.* ***B*** *represents the reaction after 50 minutes with no product formed and the dopamine beginning to decompose, seen by peak doubling. See Methods for details of the gradient.*

The HPLC chromatograms of phosphate and maleic acid buffers showed a large, broad peak in the beginning of the run which was attributed to the high amount of buffer (Figure 6). Initially, this large peak interfered with the accurate measurement of important peak areas. To resolve this, in future experiments reported in later chapters, the mobile phase was held at 0% acetonitrile for 1.0 minute before beginning the acetonitrile gradient. Although the signal to noise ratio is 4 times better at 225 nm than 280 nm, the intensity of the solvent peak is reduced by observation of 280 nm which will allow for more accurate quantitation of peak areas.

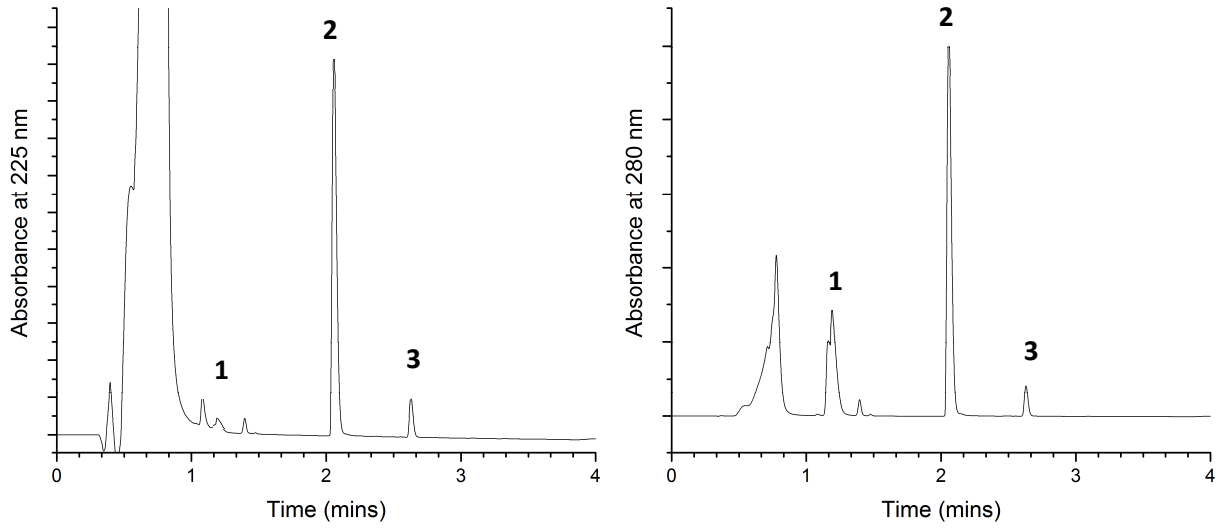

*Figure 6. HPLC chromatogram of the kinetic reaction of dopamine **1** and propanal in 80 mM maleic acid at pH 6.60 to yield tetrahydroisoquinoline **2** and iso-tetrahydroisoquinoline **3** at an absorbance of 225 nm and 280 nm.*

Conclusion

HEPES, BES, imidazole and maleic acid buffer were compared to phosphate buffer where it was determined that all the buffers except maleic acid were too slow to accurately monitor the reaction. While analyzing the buffers, a side product, isoTHI, was identified. Maleic acid buffer will be compared to phosphate buffer to determine if there is phosphate specificity for the Pictet-Spengler reaction. In order to analyze the kinetic data, area extinction coefficients will need to be determined for each of the species by applying the Beer-Lambert Law.

Chapter 3 – Determination of Area Extinction Coefficients

3.1 Introduction

The concentrations of the species in all reaction solutions need to be precisely controlled and quantifiable to draw meaningful conclusions from the effect they have on reaction rate. In HPLC-UV, the transmitted light is measured by a photodetector. Dopamine, tetraisohydroquinoline (THI), and isoTHI have aromatic chromophores that allow for their identification when using UV-light absorption. This signal is converted to a logarithmic relationship that is proportional to concentration. The logarithmic relationship is known as the Beer-Lambert Law.

$$A = log\left(\frac{I_o}{I}\right) = \varepsilon bc \qquad \textit{Eq. 1}$$

Where I is the transmitted light intensity, I_o is the incident light intensity, ε is the molar extinction coefficient, b is the path length, and c is the molar concentration of the substance. The Beer-Lambert Law allows us to determine the concentration once the extinction coefficient is known.

In HPLC-UV chromatography, the area under a peak at a given wavelength may be converted to concentration if the area-extinction coefficient (α) is known:

$$C_x = \frac{\alpha_{x\lambda} \times Area_\lambda}{b} \qquad \textit{Eq. 2}$$

Typically, extinction coefficients are measured from a linear standard curve made from standard solutions of known concentration. This was done for dopamine; however, we were not able to isolate pure samples of THI and isoTHI. Instead, we were able to determine the concentrations of the product species by completely converting a known concentration of dopamine into pure THI. The area-extinction coefficient of THI and isoTHI was then determined by a similar method.

All reactions were monitored under pseudo-first order conditions such that the concentration of propanal was very large with respect to dopamine and buffer. The excess of propanal ensures that its concentration change will not be significant during the course of its reaction with dopamine to form THI and isoTHI. Pseudo-first order conditions with propanal in excess eliminate the requirement for monitoring change in propanal concentration. Moreover, a high excess of aldehyde promotes complete consumption of dopamine by pushing the reaction equilibrium toward complete conversion to product. Furthermore, since propanal has a small molar extinction coefficient, it is difficult to follow accurately.

3.2 Methods

The accuracy and precision of these experiments were achieved by calculating the exact amount of phosphate or maleic acid and NaCl for each molarity and pH. To make sure that the pipette was delivering the correct amount of solution, they were calibrated before each run. The water used for all reactions was purified to a resistivity of 18.2 MΩ·cm (25 °C) using an EMD Millipore Ultrapure Milli-Q

reverse osmosis water purification system outfitted with ion exchange and organic removal cartridge filters.

Standard solutions

A standard 20.0 mM dopamine solution was prepared by gravimetrically measuring 94.3 mg of dopamine-HCl (MW 189.64) and dissolving to a final volume of 25.0 mL in water. A solution of 200.00 mM phosphate buffer was prepared by gravimetrically measuring 6.0 g of NaH_2PO_4 and dissolving to a final volume of 200.00 mL in water. Commercially obtained propanal (Sigma-Aldrich) was found to be contaminated with propionic acid, a product reaction with molecular oxygen. All propanal was distilled from $CaCl_2$ to remove impurities. Standard solutions of propanal were prepared by measuring the mass of propanal and diluting into volumetric glassware.

Measurement of THI and isoTHI area extinction coefficients, Method A

The THI area extinction coefficient was determined indirectly by monitoring the Pictet-Spengler reaction. From the 20.0 mM dopamine stock solution, 126.8 µL was pipetted into a separate vial. To this vial, 142 µL of 200 mM phosphate buffer and 220.3 µL of 2,270 mM stock propanal solution were mixed to a final volume of 500 µL. The final concentrations were 0.500 mM dopamine, 100 mM phosphate buffer, and 100 mM propanal, in a final volume of 500 µL. With propanal in excess and dopamine the limiting reagent, we monitored the reaction by HPLC, ensuring that the only species left in the mixture, would be the product, THI. The area under the peaks in the 225 nm chromatogram was plotted against the known concentrations.

The initial dopamine concentration was measured from identical samples prepared without aldehyde. The reactions were monitored as the reaction went to completion and the initial dopamine concentration was also determined by non-linear regression analysis using Origin software (OriginLab Corp.) to extrapolate the kinetics curve to time zero. The initial dopamine concentrations from this complimentary method were averaged equally with the concentrations from the aldehyde free controls. Once the reaction was complete, each of the reaction samples were injected five times. The area extinction coefficient of THI was determined by assuming that the final concentration of THI was equal to the initial dopamine concentration in this reaction that went to completion and the concentration of isoTHI was equal to the concentration of dopamine minus the concentration of isoTHI (Eq.3).

Next, the isoTHI extinction coefficient was determined by applying Equation 3 to complete time course datasets of reactions in both phosphate and maleate buffers. This equation assumes that the sum of all observed species at any time point must be equal to the initial dopamine concentration.

$$[Dopamine_{initial}] = \alpha_{DOP225} \times Area_{DOP225} + \alpha_{THI225} \times Area_{THI225} + \alpha_{isoTHI225} \times Area_{isoTHI225}$$

Eq. 3

For this method, the area extinction coefficients for dopamine and THI were fixed as known constants. The area extinction coefficient for isoTHI was the only unknown.

Simultaneous measurement of THI and isoTHI area extinction coefficient, Method B

The extinction coefficients of THI and isoTHI were determined indirectly by running the Pictet-Spengler reaction at low concentrations of buffer to generate a significant amount of the isoTHI side-product in solution.

The area extinction coefficient of THI was determined by preparing a 2.0 mM dopamine stock solution by adding 189.5 mg of dopamine hydrochloride to 500 mL. From the 2.0 mM dopamine stock solution, 50 mL was then added into eight 200 mL volumetric flasks. A 400 mM stock solution of propanal was prepared and diluted to 100 mM by adding 80 mL to each of the eight flasks using a volumetric pipet. Various volumes of 1.00 M phosphate stock solution were added to five of the eight flasks resulting in final phosphate buffer concentrations of 5 mM, 25 mM, 50 mM, 100 mM and 400 mM, where the other three flasks were controls. The controls contained 2.0 mM dopamine and 1.0 M propanal, without the phosphate buffer to verify that the reaction needed phosphate buffer to produce THI and isoTHI. Since no reaction was observed in the controls, they simultaneously provided a direct measurement of dopamine concentration present in the reactions and demonstrated that phosphate buffer is needed to make THI and isoTHI. The reaction in each flask was monitored via HPLC.

The extinction coefficients (α) for THI and isoTHI were then determined simultaneously by fitting the experimentally measured areas of THI ($Area_{THI225}$) and isoTHI ($Area_{isoTHI225}$) to Equation 3 using non-linear least-squares fitting in the Origin (OriginLab Corp.) to find the best parameters for both extinction coefficients. A total of 56 time points (each with different concentrations of dopamine, THI, and isoTHI) and the average of 10 initial dopamine controls were used.

3.3 Results and Discussion

After plotting the results of the dopamine standard, the dopamine extinction coefficient was determined to be $2.5\underline{6} \pm 0.02 \times 10^{-4}$ $\mu M \mu V^{-1} s^{-1}$ (Figure 7). The trend line fit the data well; in fact the correlation coefficient was 1.0. The measurement of the dopamine area extinction coefficient was straightforward, but the THI and isoTHI analysis proved to challenging. Due to certain limitations, isoTHI and THI were unable to be isolated as pure compounds for extinction coefficient determination. Their high polarity made it difficult to separate by silica column chromatography. Preparative HPLC was attempted but the volume of the isolated oils was too small for accurate mass measurement and no fractions were pure enough to definitively assign the identity of isoTHI by NMR. When analyzing the reactions, it was observed that low phosphate buffer concentration resulted in a higher ration of isoTHI side-product to THI product.

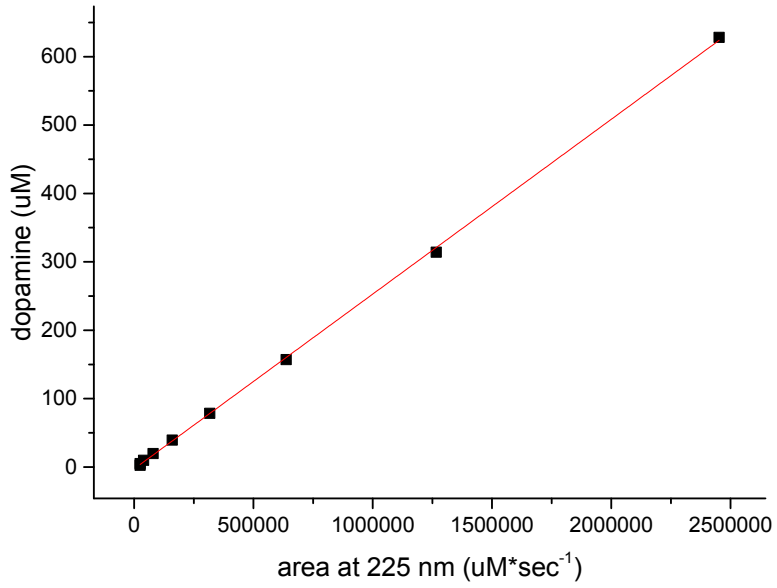

Figure 7. Dopamine area-extinction coefficient standard curve where the line of best fit is y= (2.56 ± 0.02) x 10^{-4} μMμ$V^{-1}s^{-1}$ x – 2.7 ± 1 μM and R^2=1.0.22

Method A

The observation that high phosphate concentration reduces the production of isoTHI was used to determine the THI extinction coefficient through quantitative conversion of a known stock solution of dopamine to THI in the presence of high phosphate. The resulting THI extinction coefficient was then used along with the dopamine extinction coefficient to derive the isoTHI extinction coefficient from existing raw kinetics data in both phosphate and maleic acid buffers. The concentrations of dopamine and THI were first determined by multiplying their extinction coefficients, determined by the raw data from the kinetic runs, by application of Equation 2. Next, Equation 3 was applied to dozens of full kinetics datasets to determine the area extinction coefficient for isoTHI ($\alpha_{isoTHI225}$) setting the other two area extinction coefficients, α_{DOP225} and α_{THI225}, as fixed parameters. It was assumed that the THI area extinction coefficient values were accurately measured. From this, we extracted the isoTHI values based on the assumption that the area of dopamine, THI, and isoTHI should always be constant. For reasons that are still unclear, this method (Method A in the Methods section of this chapter) yielded a different $\alpha_{isoTHI225}$ value for every dataset. The values are different by orders of magnitude. This method (Method A) gave an extinction coefficient of 2.26 ± 0.02 x 10^{-4} μMμ$V^{-1}s^{-1}$ for THI and 2.22 ±0.88 x 10^{-4} μMμ$V^{-1}s^{-1}$ for isoTHI. The estimated error in the THI extinction coefficient is an order of a magnitude smaller than that of isoTHI. One possible explanation for the discrepancies could be that the area extinction coefficient for THI was not initially determined correctly due to small amounts of unreacted dopamine or isoTHI present in the samples. Therefore, a second method was developed to circumvent this problem.

Method B

For this second method (Method B in the methods section), the volumes of all reactions were larger (200 mL versus 500 μL) to minimize errors due to pipetting and evaporation of the aldehyde. A series of six time course experiments were set-up, each with a different phosphate buffer concentration. Since

the relative rates of the competing reactions are dependent on phosphate concentration, the ratios of THI to isoTHI were variable such that Equation 3 could be used to determine two constants, α_{THI225} and $\alpha_{isoTHI225}$, from non-linear least squares fitting using Origin graphing and analysis software (OriginLab Corp.). By using the extinction coefficient of dopamine as $2.56 \times 10^{-4} \pm 1 \times 10^{-6}$ $\mu M \mu V^{-1} s^{-1}$, the concentration of dopamine from each sample reaction was plotted versus the area of THI from the each of the reactions, and then isoTHI. By applying Equation 3, the extinction coefficients were determined to be $2.146 \pm 0.005 \times 10^{-4}$ $\mu M \mu V^{-1} s^{-1}$ for THI and $2.34 \pm 0.07 \times 10^{-4}$ $\mu M \mu V^{-1} s^{-1}$ for isoTHI. Although determined indirectly, the extinction coefficients demonstrate a high level of confidence (Table 2).

Table 2. Comparison of extinction coefficients for THI and isoTHI.

Method	THI, $\mu M/\mu V/s$	T-value	isoTHI, $\mu M/\mu V/s$	T-value
A	$2.26 \pm 0.02 \times 10^{-4}$	1.01	$2.22 \pm 0.9 \times 10^{-4}$	18.08
B	$2.146 \pm 0.005 \times 10^{-4}$		$2.34 \pm 0.07 \times 10^{-4}$	

Conclusion

Determining the extinction coefficients of the species of the Pictet-Spengler reaction will allow us to quantify the peak areas from the HPLC plots. The extinction coefficients for dopamine, THI and isoTHI were determined first by using a method that extracted the extinction coefficients from the kinetic data sets. However, some of this data had very low isoTHI concentrations thus prone to error. Method B ran a set of controlled kinetics experiments that were designed to give larger isoTHI peaks. Two different sets of extinction coefficients were determined (Table 2). A t-test was calculated to determine if the two method results are significantly different. It was found that at a 95% confidence, the THI values are not significantly different within the stated uncertainties; where the t-value of 1.01 is less than the standard t-value of 2.228 for method A and 2.004 for method B. The isoTHI extinction coefficient values are statistically different with a t-value of 18.08 where the standard t-value for method A is 2.12 and 2.00 for method B. [23] Because it was determined that there is statistical difference between the two methods, method B extinction coefficients were applied for the kinetic analysis to further understand the Pictet-Spengler mechanism. The extinction coefficients for dopamine, THI and isoTHI were determined to be $2.56 \times 10^{-4} \pm 1 \times 10^{-6}$ $\mu M \mu V^{-1} s^{-1}$, $2.146 \pm 0.005 \times 10^{-4}$ $\mu M \mu V^{-1} s^{-1}$ and $2.34 \pm 0.07 \times 10^{-4}$ $\mu M \mu V^{-1} s^{-1}$, respectively. These values will be applied to the kinetic data sets in order to analyze the data and clarify the role of phosphate in the Pictet-Spengler reaction. In addition, the role of buffers in the reaction will be examined to understand the Pictet-Spengler mechanism.

Chapter 4 - HPLC kinetics and Analysis of Time Course Data

4.1 Introduction

Catalysis in the Pictet-Spengler Reaction

Catalysis by buffers plays a significant role in this reaction. Understanding the specific reaction steps catalyzed by buffer will help elucidate the function of phosphate in the mechanism of this Pictet-Spengler reaction. Previous work has shown that aqueous Pictet-Spengler reactions of the indole tryptamine with propanal depend on acid catalysis.[24] Determination of the separate rate constants for buffer-catalyzed acid and base catalysis should also reveal whether or not the apparent phenomenon seen for phosphate catalysis is really just a function of the concentration of the catalytic species, which will be different for two buffers of different pKas at the same pH.

The general second order rate constant, k_{obs}, for a two substrate reaction is given in Eq. 4.

$$Rate = k_{obs}[Dopamine][Aldehyde] \qquad \text{Eq. 4.}$$

The contributions of all possible general acid and base catalysts may be described as follows.

$$k_{obs} = k_1[H^+] + k_2[OH^-] + k_a[BH^+] + k_b[B] + k_3 \qquad \textit{Eq. 5.}$$

These five rate constants represent the contributions of specific acid catalysis (k_1), specific base catalysis (k_2), general acid catalysis (k_a), general base catalysis (k_b), and the rate of the uncatalyzed reaction (k_3) respectively.

The Pictet-Spengler reaction with dopamine and aldehyde is both acid and base catalyzed in buffer (Scheme 7). If this reaction is specifically acid-base catalyzed, the buffer concentration will not have an effect on the reaction; whereas, if the reaction is general acid-base catalysis, the rate of the reaction will be dependent on the buffer concentration. Step 1 of the reaction may be acid or base catalyzed due to the pKa of the amine (9-10). At the pH levels that are being studied, the amine will most likely be charged. Therefore, the amine in the first step is the dominant equilibrium species. The pKa of the protonated ketone is roughly 6; so acid catalysis by the protonating ketone is less likely than deprotonation of the amine. This indicates that there is most likely a base-dependent step before step 1. Step 3 is a tautomerization reaction which requires both acid and base. The **~H$^+$** in step 3 shows that H$^+$ is effectively hopping from one part of the molecule to another. In reality, a proton cannot make such a hop in one step because such a reaction would be a [1,3] sigmatropic shift. This is not feasible because the transition state is impossible to achieve by Woodward-Hoffmann rules. There are two possibilities in step 3, either first a base deprotonates then an acid protonates or first an acid protonates and then a base deprotonates. Both are likely to be occurring. Both are fast steps when both acids and bases are present (as is the case in a buffer). Both paths are kinetically equivalent and indistinguishable. In addition, tautomerization is generally not rate limiting in imine formation.[25]

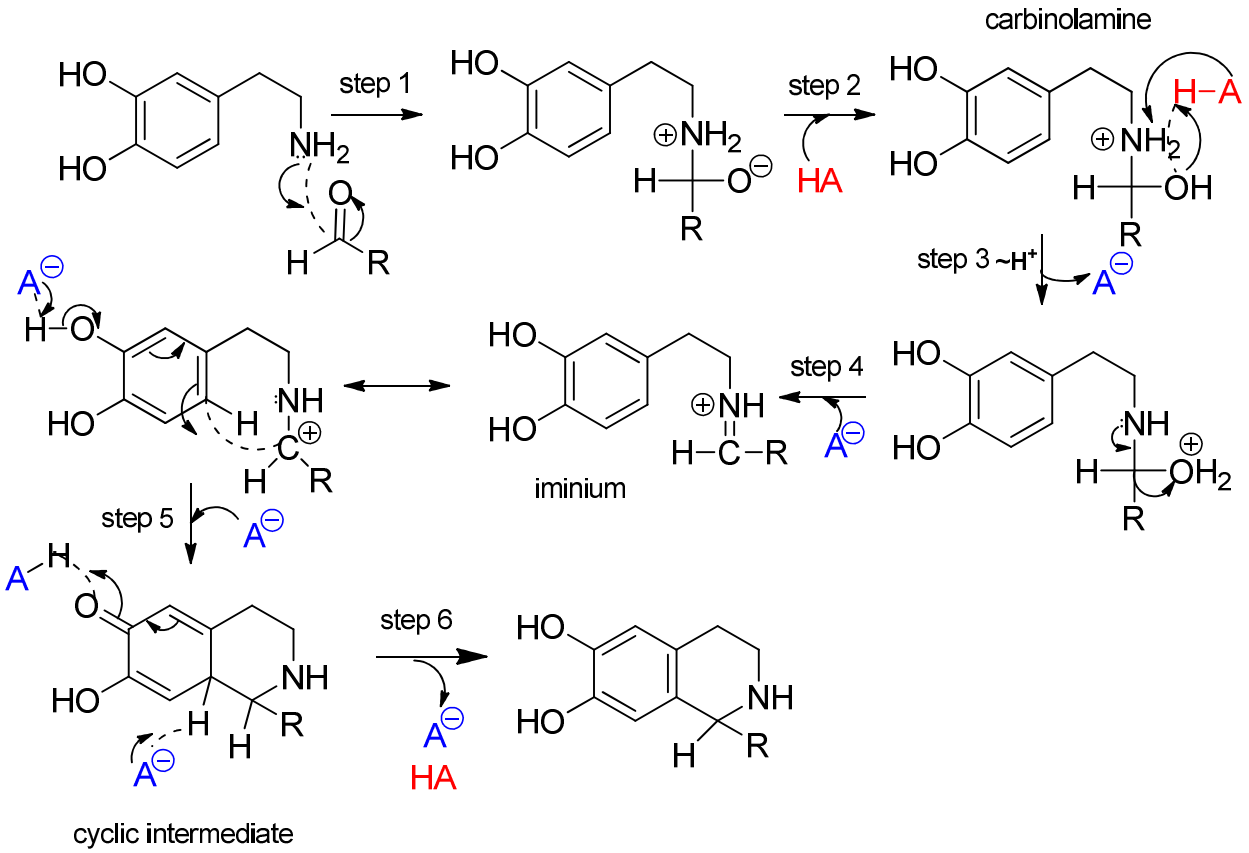

Scheme 7. Pictet-Spengler Reaction in both acid and base catalyzed buffer. In step 1, aldehyde undergoes nucleophilic attack by an amine from dopamine. In step 2-4:proton transfer results in the release of water, resulting in a protonated imine intermediate. In step 5, a 6-endo-trig cyclization reaction occurs with a loss of aromaticity. Finally in step 6, deprotonation reestablishes aromaticity, resulting in tetrahydroisoquinoline product. (Red colored or blue colored molecules signify acid or base catalyzed steps, respectively.

One method to determine the values of these constants is to measure k_{obs} as a pseudo-first order rate constant at constant pH and ionic strength while varying the total buffer concentration (B_t). The dependence of the reaction on buffer catalysis can be analyzed by simplifying Eq. 5 based on the fact that, k_o in Eq. 6 is constant when pH is constant.

$$\mathrm{k_o} = \mathrm{k_1[H^+]} + \mathrm{k_2[OH^-]} + \mathrm{k_3} \qquad \textit{Eq. 6}$$

Since [BH^+] and [B] are related to [H^+] and B_t as

$$F_B = \frac{[B]}{B_t} = \frac{K_a}{K_a + [H^+]} \qquad \textit{Eq. 7}$$

and

$$F_{BH} = \frac{[BH^+]}{B_t} = \frac{[H^+]}{K_a + [H^+]} \qquad \textit{Eq. 8}$$

where K_a *is the acid dissociation constant of* BH^+*, Eq. 5 can be expressed as*

$$k_{obs} = k_o + (k_b F_B + k_a F_{BH}) B_t \qquad \textit{Eq. 9}$$

Thus, the relationship of total buffer concentration at constant pH is linear. Since $F_B + F_{BH} = 1$, Eq. 9 can be written in terms of the conjugate base as

$$k_{obs} = k_o + \left(k_b F_B + k_a (1 - F_B)\right) B_t = k_o + (k_a + (k_b - k_a) F_B) B_t \qquad \textit{Eq. 10}$$

This equation can be rearranged into the form

$$\frac{k_{obs} - k_o}{B_t} = k_a + (k_b - k_a) F_B \qquad \textit{Eq. 11}$$

A plot of $\frac{k_{obs} - k_o}{B_t}$ versus F_B will then be linear. The y-intercept of the plot is equal to k_a; the value of y at $F_B = 1$ is equal to $k_b - k_a$; knowing k_a from the y-intercept then allows k_b to be determined.

Using this method to determine k_a and k_b will allow us to determine the relative contributions of the conjugate acid and conjugate base species from the buffer. If either the conjugate acid or conjugate base plays a greater role in catalysis, this narrows down which species participates in the critical rate limiting step of the reaction. This can also help us to eliminate steps in the reaction (Scheme 7) that are not rate limiting in the mechanism. Comparing the catalytic effects of different buffers should contribute to a greater understanding of the specific role played by phosphate in catalysis of this reaction. For example, phosphate may accelerate the rate of one step to such an extent that the rate limiting step changes. Additionally, it may be revealed that the differing pKa of the buffers is the major contributor to their different activities. For example, if k_b is rate limiting and essentially identical for two different buffers, then we could conclude that the apparent advantage of one buffer over the other at a given pH and identical B_t is merely the concentration of [B] and not a feature of the catalyst itself.

The Curtin-Hammett Principle

The Curtin-Hammett principle is often applied in chemical kinetics to understand the mechanism. By first establishing the relationship between the concentrations of reactants, catalysts and rate, we can then vary the other conditions to learn about the mechanism. In the following figure, (Figure 8), two reactants react to form two different products, just like in the Pictet-Spengler reaction with aldehyde and dopamine.

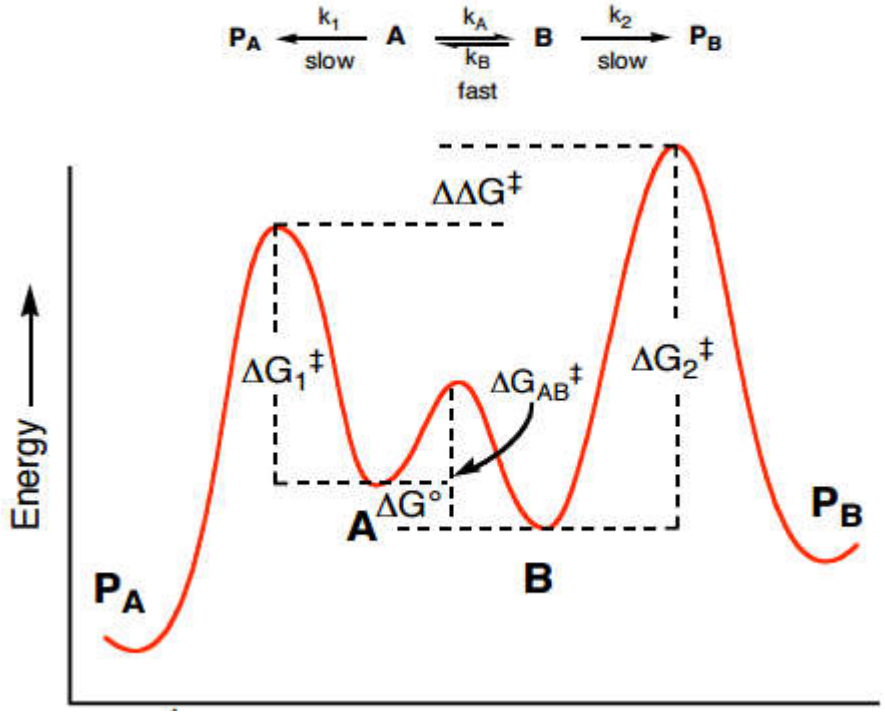

Figure 8. Reaction coordinate free energy profile where A and B reactants react to form two products, P_A and P_B.

Similarly, in this reaction we see the formation of two products, THI and isoTHI. The rate equations for this reaction will be, where *[A]* is the concentration of THI and *[B]* is the concentration of isoTHI.

$$\frac{d[P_A]}{dt} = k_1[A] \text{ and } \frac{d[P_B]}{dt} = k_2[B] \qquad \textit{Eq. 12}$$

The rate equations can then be combined to form:

$$d[P_B] = \frac{k_2[B]}{k_1[A]} d[P_A] \qquad \textit{Eq. 13}$$

Because *A* and *B* are in equilibrium, we apply $K_{eq} = \frac{[B]}{[A]}$ to form:

$$d[P_B] = \frac{k_2}{k_1} K_{eq} d[P_A] \qquad \textit{Eq. 14}$$

And by integrating we get:

$$[P_B] = \frac{k_2}{k_1} K_{eq} \qquad \textit{Eq. 15}$$

Recall that $K_{eq} = e^{-\Delta G^\circ/RT}$, $k_1 = e^{-\Delta G_1 ‡/RT}$ and $k_2 = e^{-\Delta G_2 ‡/RT}$ which can then be substituted into Eq. 15 to give the Curtin-Hammett principle.

$$\frac{[P_B]}{[P_A]} = \frac{e^{-\Delta G_2 ‡/RT}}{e^{-\Delta G_1 ‡/RT}} e^{-\Delta G^\circ/RT} = e^{-\Delta\Delta G^‡/RT} \qquad \textit{Eq. 16}$$

By applying the Curtin-Hammett principle to this reaction (Equation 17) we can make predictions about reaction rate constants for a reaction from free-energy relationships. As seen in Eq. 17, the product ratio depends on the difference in free energy on the transition state leading to the products where $\Delta\Delta G^‡$ is the change in the free energy, R is a gas constant, and T is temperature. [26]

$$\frac{[THI]}{[iso-THI]} = e^{\Delta\Delta G^‡/RT} \qquad \textit{Eq. 17}$$

4.2 Methods

The reactions were conducted close to pH 7.0 and a series of constant ionic strength buffers were prepared using the Debye-Hückel equation described by Ellis[27] using *A* = 0.509 for 25°C.

$$p\mathrm{Ka}^* = pKa + (2z+1)\left[\frac{0.509\, I^{1/2}}{1 + I^{1/2}} - 0.1I\right] \qquad \textit{Eq. 18}$$

For phosphate buffer (practical pKa of 6.84), the constant ionic strength was 0.10 M. A 100 mM stock solution of sodium phosphate (NaH_2PO_4) that was diluted for the 10 mM, 20 mM, and 40 mM samples and for each of the pH values of 6.60, 6.90, and 7.20. A, constant ionic strength was obtained by adjusting with NaCl.

The reactions were monitored via HPLC-UV as described in Chapter 3 with the ambient temperature of the autosampler compartment maintained at 23.00 °C. All reactions were conducted under pseudo-first order conditions with the starting concentration for dopamine and propanal as 0.500 mM and 100 mM

respectively. The extinction coefficients from Chapter 3 were applied to determine the concentrations of dopamine, THI, and isoTHI at each time point. The times for the observed concentration data were adjusted with a time delay correction of 50 seconds to correct for the delay between the timestamp of the data file and the actual start of the run.

The raw data was plotted in Origin by exponential fit to extrapolate a starting value for dopamine's starting concentration. This starting concentration of dopamine was then included with the rest of the data and simulated in Gepasi. The Gepasi software program[28] [28c]was then used to estimate the pseudo-first order kinetic constants k_{thi} and k_{isoTHI} from a model of dopamine reacting with THI (Eq. 13) and isoTHI (Eq. 14) by non-linear least squares fitting of the experimentally measured dopamine, THI, and isoTHI concentrations at all measured time points. In Gepasi, the reaction was defined as a mass action reaction that is irreversible, where dopamine makes either THI or isoTHI. A genetic algorithm using 500 generations and a population of 10 gave the lowest sum of squares deviation and was used as the parameter search method for all experiments.[28a]

$$Dopamine \xrightarrow{k_{thi}} THI \qquad \textit{Eq. 19}$$

$$Dopamine \xrightarrow{k_{isoTHI}} isoTHI \qquad \textit{Eq. 20}$$

Three parameters, k_{thi}, k_{isoTHI}, and the initial dopamine concentration, were optimized to the experimental time course data. The initial product concentrations were set to zero. The initial dopamine concentration was permitted ±10% variance to account for possible pipetting errors. The pseudo first order rate raw data was converted to second order rates constants by dividing by the aldehyde concentration.

4.3 Results

A series of reactions were carried-out with starting concentrations of 0.500 mM dopamine and 100 mM propanal. The phosphate buffer concentration was varied in such a way that three different pH values (6.6, 6.9 and 7.2) and three different total phosphate concentrations (10 mM, 20 mM, and 40 mM phosphate buffer) were tested. The area extinction coefficients from Method B of Chapter 3 were used to convert peaks areas observed in HPLC time course data to concentrations. These concentrations were fit to a kinetic model of two competing irreversible reactions using the Gepasi software program. Figure 9 shows the quality of a representative fit by plotting concentrations with time based on the estimated parameters and the experimental data.

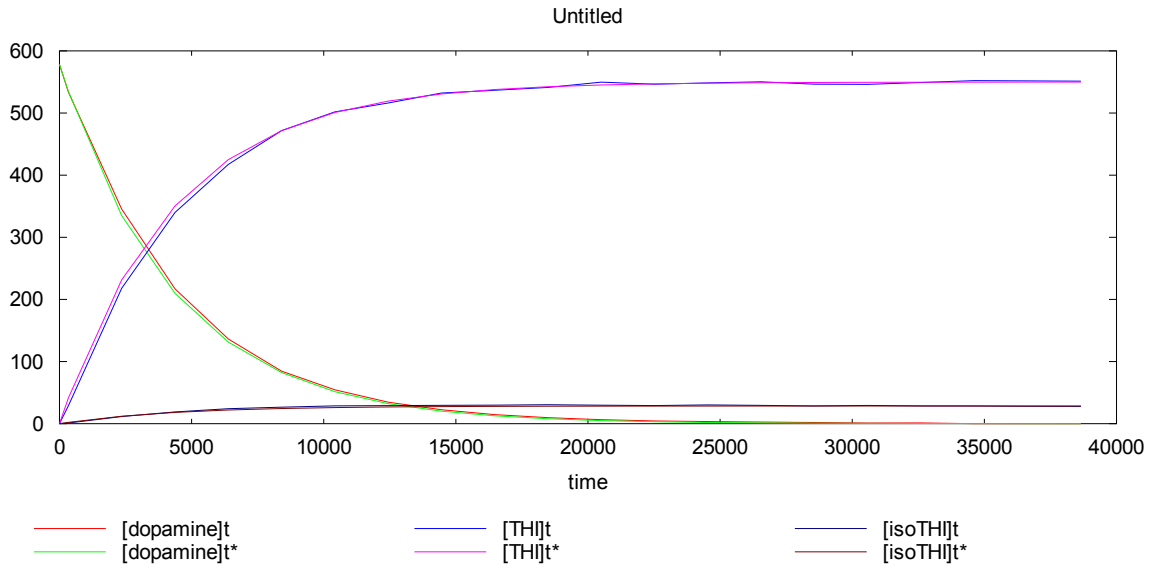

Figure 9 Gepasi parameter estimation of Pictet-Spengler reaction in 40 mM maleic acid buffer at a pH of 6.11. ***concentration of dopamine*** ***predicted concentration of dopamine,*** ***concentration of THI,*** ***predicted concentration of THI,*** ***concentration of isoTHI,*** ***predicted concentration of isoTHI.***

General Base Catalysis

The results of all nine pH and buffer concentration trials are shown in Figure 10, where the rates have been converted to second order rate constants by dividing by the aldehyde concentration. General base catalysis is observed in this Pictet-Spengler reaction where the rate of the reaction depends on concentration of buffer. It was observed that the phosphate buffer reaction was dependent on both pH and concentration of buffer. At a constant pH, the rate is proportional to the concentration. Similarly, at a constant concentration, the rate increased as the pH increased. The observed trend for this data is most likely due to the increase of the hydroxide species. As the pH of the phosphate buffer decreases to 6.6, the amount of hydroxide species decreases and reaches the buffering capacity of phosphate buffer, thereby slowing the reaction. This is indicative of general buffer catalysis.

If specific acid catalysis was observed, the rate of reaction would be independent of the concentration of buffer, due to the rate dependence on the concentration of the hydronium ion. The constituents of the buffer have no effect on the rate other than establishing the pH of the solution.

Although there are only three data points for each concentration/pH trial and a linear trend is shown, three data points do not make a trend. In this case, however, each of these data points are actually derived from hundreds of concentrations and times. In the future, more buffer concentrations and pH values will need to be acquired to verify the trends that are suggested.

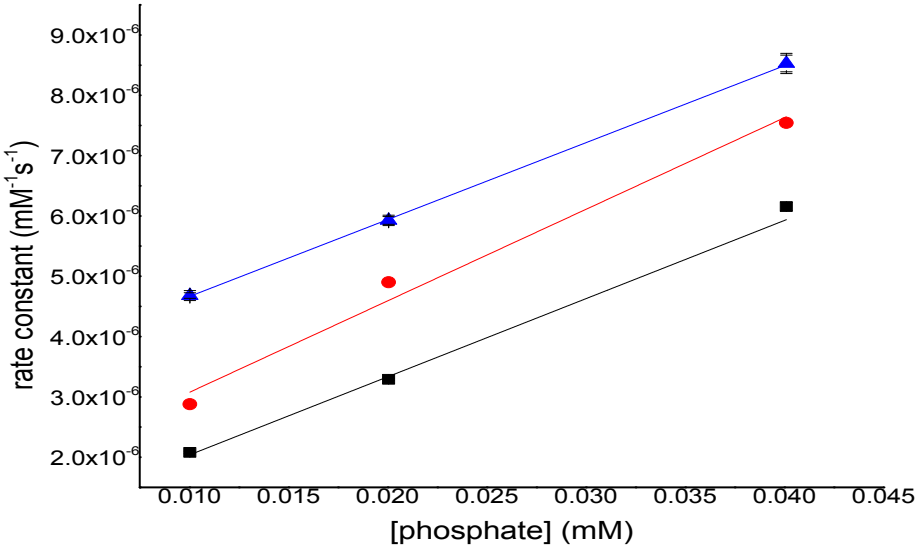

Figure 10. Observed rate constant dependence as a function of phosphate buffer for the reaction of dopamine at a constant concentration with pH increasing, producing THI. (■) pH 6.6 :Linear regression results give a relationship of k_{obs} = 1.30 ± 0.09 x10^{-4} mM^{-1}s^{-1}mM^{-1} x + 7.4 ± 2 x10^{-7}mM^{-1}s^{-1} where R² = 1.0 (●)pH 6.9: Linear regression gives a relationship of k_{obs} = 1.52 ± 0.2 x10^{-4} mM^{-1}s^{-1}mM^{-1} x + 1.56± 0.5 x10^{-} mM^{-1}s^{-1}and R² = 0.99 (◢) pH 7.2: Linear regression gives a relationship of k_{obs} = 1.275 ±0.02 x10^{-4} mM^{-1}s^{-1}mM^{-1} x + 3.389 ±0.04 x10^{-6} mM^{-1}s^{-6} and R² = 0.998.

Curtin-Hammett Principle

The calculated concentrations of products THI and isoTHI were calculated and the Curtin-Hammett principle (Eq. 17) was applied. Plotting the ratio of the concentration of THI over the concentration of isoTHI to the concentration of phosphate reveals a linear dependence correlated to total phosphate (

Figure 11). This indicates that phosphate in general is catalyzing the pathway to one product more so than the pathway to the other product. At 20mM phosphate, the data points begin to converge on a single value signifying that the ratio at this concentration are consistent at the varying pHs. However, at 10 mM and 40 mM the data points scatter, indicating that there is error within the data set and the data set trials need to be repeated to verify the trends seen. Further investigations will hopefully clarify the mechanism of this phenomenon.

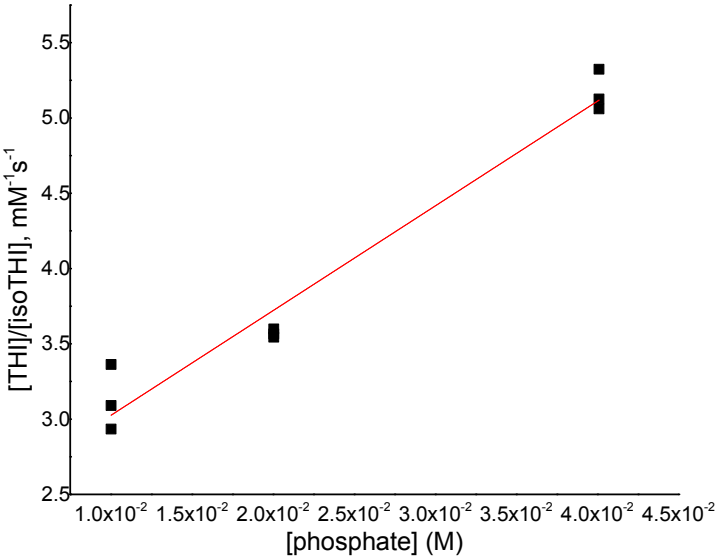

Figure 11. Rate of the concentration of THI over the concentration of isoTHI as a function of phosphate concentration. Where the line of best fit is y= 69.57 ± 5.0 mM^1s^{-1} M^{-1} x + 2.33 ± 0.10 M and R^2=0.96.

A plot of either [BH+], $H_2PO_4^-$, or [B], $H_2PO_4^{2-}$ against the [THI]/[isoTHI] ratio reveals that within a single phosphate concentration, [B] increases the relative yield of THI and [BH+] decreases the relative yield of THI (Figure 11,Figure 12,Figure 13). This suggests a role for base catalysis for the acceleration of THI formation relative to isoTHI. The factors controlling the two competing reactions will need to be investigated in more detail in a later study (see Chapter 5 for limitations encountered in this work).

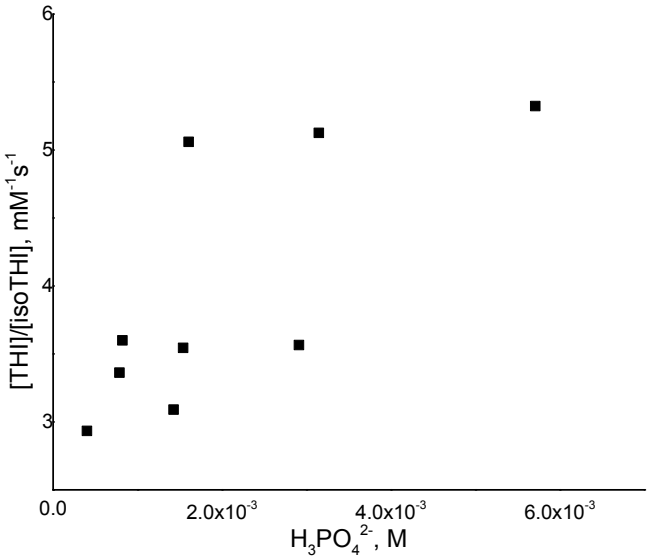

Figure 12. Rate of the concentration of THI over the concentration of isoTHI as a function of acidic species of phosphate concentration.

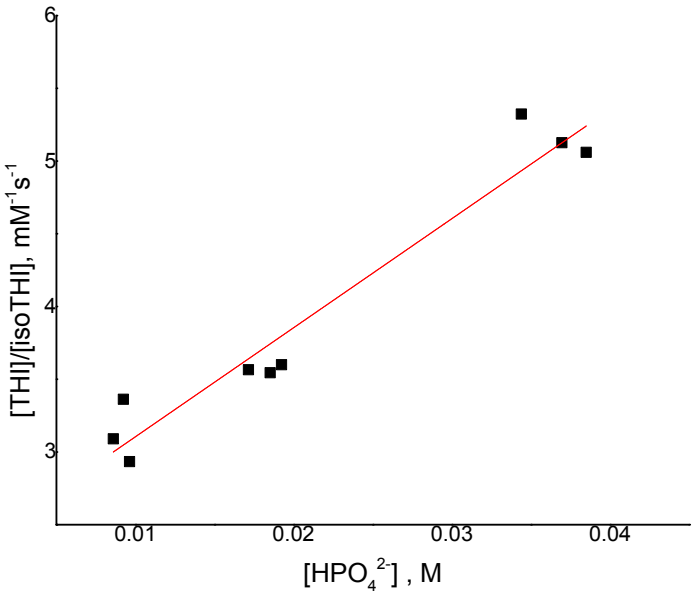

Figure 13. Rate of the concentration of THI over the concentration of isoTHI as a function of basic species of phosphate concentration

Acid/Base Catalysis

To determine if the reaction is primarily acid or base catalyzed, the data from Figure 10 was plotted as rate constant against monobasic phosphate (the conjugate acid [BH^+]) and dibasic phosphate (the conjugate base [B]) concentration to give Figure 14 and Figure 15. The results clearly show that there is no trend for acid catalysis.

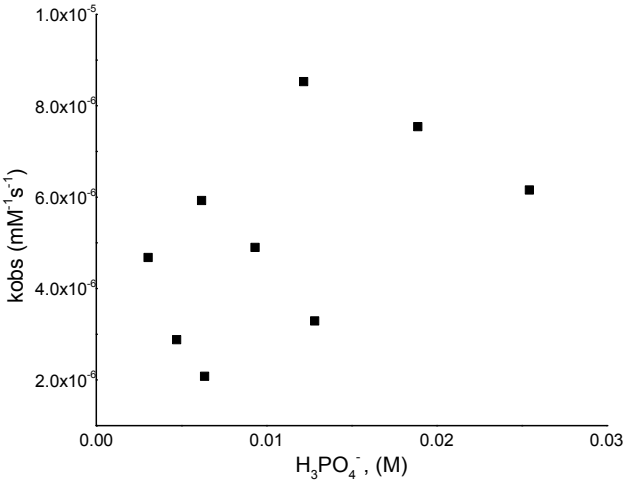

Figure 14. Observed rate constant dependence as a function of acidic species of phosphate.

The plot of the observed rate dependence on the basic species of phosphate demonstrates a linear trend. Although there appears to be a possible break at the later concentrations of the basic species of phosphate, this is not what has been observed in the raw data itself. If there was a break, the rate-limiting step would abruptly change which has not been observed in the raw data. It is more probable that these are artifacts in the data set. As mentioned before, there is scatter in the original data set (Figure 10) and the scatter will be more so pronounced when applying different conditions.

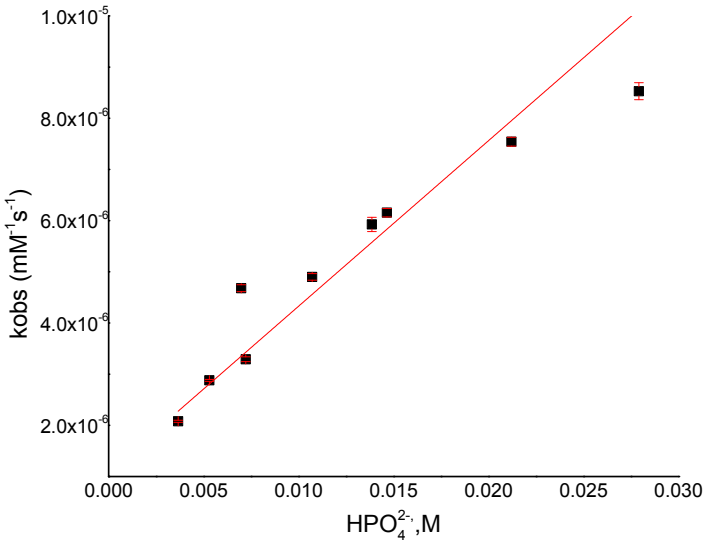

Figure 15. Observed rate constant dependence as a function of basic species of phosphate. Line of best fit y=3.3<u>5</u> ± 0.3 x 10^{-4} $mM^{-1}s^{-1}$ x + 9.<u>4</u> ± 2.3 Mx 10^{-7} and R^2=0.9<u>7</u>.

The apparent linear dependence of rate on base catalysis indicates that [BH^+] is not the rate-limiting catalytic species. Since the reaction is apparently dependent on the concentration of dibasic phosphate [B],Figure 15 describes the equation

$$k_{obs} = k' + k_b[B] \qquad \textit{Eq. 21}$$

where the y-intercept $k' = k_1[H^+] + k_2[OH^-] + k_a[BH^+] + k_3$ *for the condition of [B] = 0.*

However, in Equation 5 [B] and [BH^+] are not the only contributors to k_o. If we assume that k_2 has no dependence on the buffer, we can substitute

$$[BH^+] = [B_t] - [B] \qquad \textit{Eq. 22}$$

into Equation 23, giving,

$$k_o = k_b[B] + k_2 + k_a([B_t] - [B]) \quad \text{Eq. 23}$$

This demonstrates that both the acid catalysis rate constant and base catalysis rate constant has some dependence on [B].

General Acid/ Base Catalysis Rate Constants

The values of $\frac{k_{obs} - k_o}{B_t}$ were plotted against the fractional base (Figure 16) to determine if the conjugate acid or base contributes to catalysis. The rate constant for general acid catalysis (k_a) was calculated to be 1.52 ± 0.2× 10^{-4} $mM^{-2}s^{-1}$ and the rate constant for general base catalysis (k_b) is 1.26 ± 0.4 x 10^{-4} $mM^{-2}s^{-1}$. The rate constant for base catalysis is slower than acid catalysis, therefore suggesting that base catalysis contributes more to the mechanism. If the data had less scatter, the data points would begin to converge as seen for the data values of 0.9 M fractional base. Due to limitations, more data will need to be collected to identify and verify a trend.

If acid catalysis contributed more to the mechanism, the trend would look similar to what was seen in the tryptamine Pictet-Spengler reaction (Figure 17) where acid catalysis contributes more to the reaction. It is also hypothesized that the acid-catalyzed step becomes rate-controlling and the deprotonation step is no longer rate-limiting.[29]

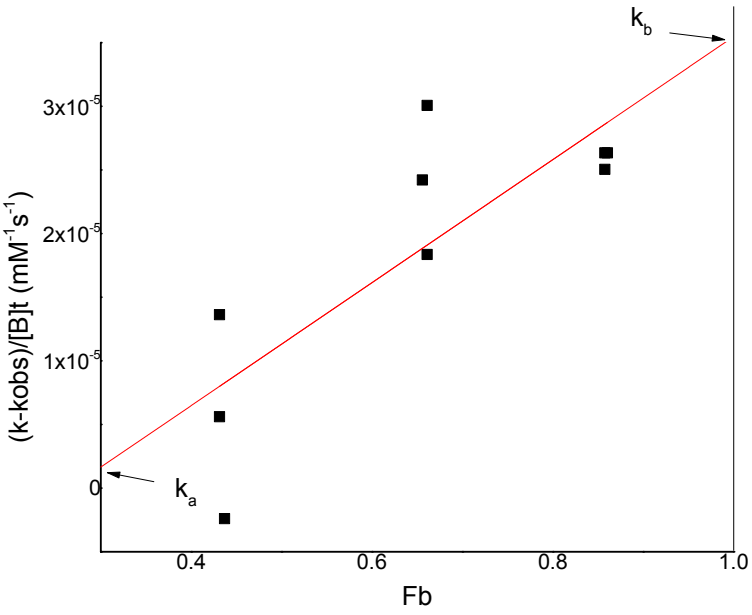

Figure 16. Dependence of $\frac{k_{obs} - k_o}{B_t}$ on fractional base of the reaction in phosphate buffer where y =-2.6± 3 x10^{-5} $mM^{-1}s^{-1}M$ x + 1.52 ± 0.2 x10^{-4} M.

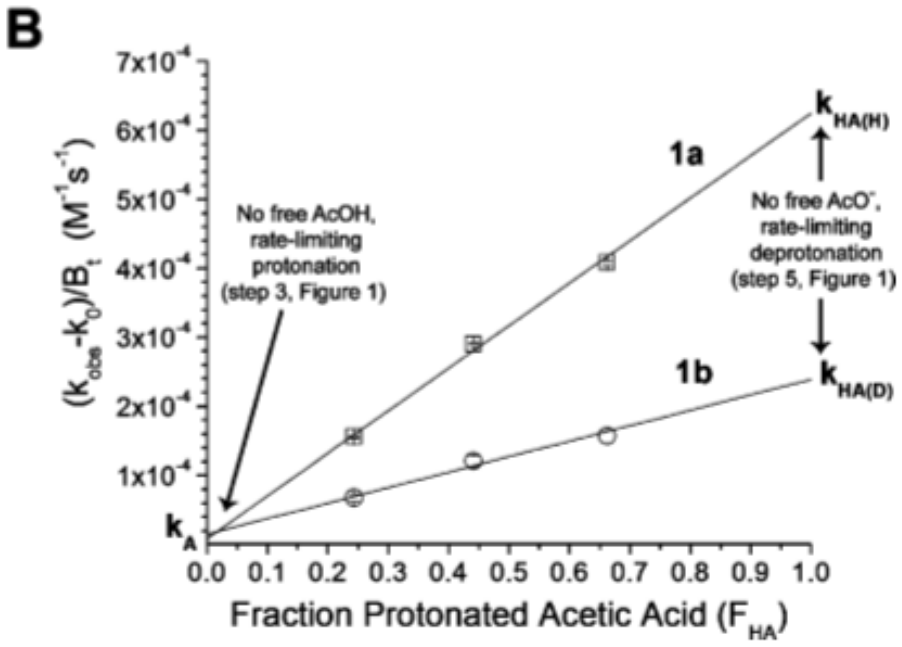

Figure 17. Pictet-Spengler reaction of tryptamine where the KIE is 1 for k_A and 2.65 for k_{HA}.[29]

Conclusions

For this experiment, the concentration of the base and pH vary. This in turn varies the base/acid ratio. The data were not clean enough to apply equation 11 to determine k_a and k_b in Figure 14. Nonetheless, the general trend toward increasing rate with increasing conjugate base in Figure 14 combined with the observation that the same data show a strong linear dependence on conjugate base concentration (Figure 13), but not conjugate acid concentration (Figure 12) qualitatively suggest that the conjugate base species from the buffer catalyzes the rate limiting step of this reaction. This is the opposite what was observed for the indole Pictet-Spengler reaction, which exhibited rate limiting acid catalysis.[29] Based on the proposed mechanism in Scheme 7, step 4 is in a base dependent equilibrium and step 5 is base catalyzed. The reaction is clearly dependent on the base concentration (Figure 15) therefore the rate limiting transition state must contain a molecule of basic phosphate. Either the rearomatization (step 6) or the electrophilic cyclization (step 5) are ideal candidates. In order to distinguish which step is the rate limiting transition state, I will examine whether the substitution of the ring hydrogen atoms for deuterium exhibits a primary kinetic isotope effect. This can also help us to eliminate steps in reaction Scheme 7 that are not rate limiting. Comparing the catalytic effects of different buffers should contribute to a greater understanding of the specific role played by phosphate in catalysis of this reaction. For example, phosphate may accelerate the rate of one step to such an extent that the rate limiting step changes.

Chapter 5 – Maleic Acid Buffer and Kinetic Isotope Effects

5.1 Introduction

To further understand the role phosphate plays in the Pictet-Spengler reaction, the role of phosphate in maleate buffer and the dependence of the rate constant on the kinetic isotope effect for deprotonation of [2,5,6-^{2}H]-dopamine was examined. The addition of the heavy isotope of hydrogen allows us to determine if removal of the deuterium/hydrogen occurs in the limiting transition state for this multi-step reaction. Observing how a kinetic isotope effect changes with different reaction conditions can provide insight into the influence of those reaction conditions on the mechanism.

When replacing hydrogen with the heavier atom (deuterium) in a reactant, the energy barrier to the transition state will be larger, thereby slowing the rate of reaction. This is known as a kinetic isotope effect. Due to a lower zero-point energy for a heavier isotope in a bond, the bond dissociation energy for C-D is greater than C-H. Therefore, the rate of reaction for a deuterated species will be slower than for the natural abundance species. The effect will only be observable if the step in which the hydrogen/deuterium is removed is the highest energy barrier (rate limiting step) in a multistep reaction coordinate diagram. If a primary isotope effect is observed, the bond broken in the rate limiting transition state is the one that has the deuterium atom. If there is a secondary isotope effect, the bond to the isotopically labeled atom is not broken or formed during the rate determining step. Instead, the hybridization state of that atom undergoes a change.[30]

We hoped that the use of deuterated dopamine (

Scheme 8) would allow us to determine the rate determining step. Typically, electrophilic aromatic substitution reactions will give a secondary isotope effect on the aromatic D/H due to the hybridization change occurring next to the heavy atom (step 5,**Error! Reference source not found.**) when ring substitution is rate limiting. A primary isotope effect is observed when the deprotonation is the rate limiting step (step 6 of Scheme 7). By determining the kinetic isotope effect, we can determine what the rate limiting step is. In addition, any change in the kinetic isotope effect with buffer concentration and pH may provide insight into the catalytic roles of those species.

Kinetic isotope effects for the chemically catalyzed Pictet-Spengler reaction of phenethylamines (like dopamine) with aldehydes have never been reported. We were interested in determining whether the reaction has a secondary isotope effect, as is typically seen in electrophilic aromatic substitutions, or a primary isotope effect.

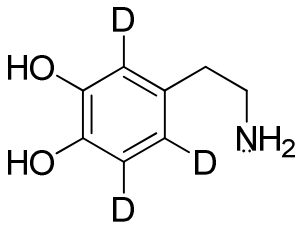

Scheme 8. Deuterated dopamine, where D is the deuterated atom, utilized to determine if there is a kinetic isotope effect.

5.2 Methods

Preparation of Maleic Acid Buffer

Maleic acid buffer was prepared in the same manner as described in Chapter 4. The practical pKa (the value at the ionic strength of the experiment) for maleic acid was calculated as 5.82 for a constant ionic strength of 0.220, the specific conditions of the experiment. The constant ionic strength of maleic acid was maintained at 0.220 M at 25 °C with B_t at either 20 mM, 40 mM, or 80 mM and pH at either 5.70, 6.10, or 6.60.

Preparation of [2,5,6-^{2}H]-dopamine.

The deuterated dopamine was synthesized as previously described in Vinning et. al[26]. Commercial dopamine hydrochloride (10 mg) was added to a sealed 48 mL high-pressure reaction tube (Ace Glass 8648 Pressure Tube with PFTE-glass plunger valve) along with 1.0 mL of 99.99% D_2O (Isotech Labs). The tube was sealed and the liquid was frozen in liquid nitrogen. The tube was attached to a freeze dryer (Labconco FreeZone 1) and evacuated for 20 minutes at 0.050 Torr. The tube was sealed and placed in a 190 °C oven for 24 hours. The excess solvent was removed *in vacuo* on a Büchi RotoVapor in a 40 °C water bath. The resulting white crystalline solid had ^{1}H-NMR spectra identical to natural abundance dopamine, but with no aromatic or phenol protons. *[2,5,6-^{2}H]*-dopamine: ^{1}H NMR (300 MHz, $CDCl_3$) δ 3.09 (t, *J* = 7.6 Hz, 2H), 2.79 (t, *J* = 7.6 Hz, 2H).

Dopamine: ^{1}H NMR (300 MHz, $CDCl_3$) δ 2.64 – 2.58 (m, 2H), 2.56 (dd, *J* = 3.1, 0.8 Hz, 1H), 1.20 (t, *J* = 7.6 Hz, 2H), 1.09 (t, *J* = 7.6 Hz, 2H).

High Resolution Mass Spectrometry

High resolution mass data (HRMS) were obtained on a Waters SYNAPT G1 High Definition Mass Spectrometer using an ESI ionization source in positive mode with HPLC separation on Waters Acquity XBridge BEH C18 column (5 µm, 2.1x100 mm); 0.4 mL/min; 0-70% acetonitrile in 0.1 % trifluoroacetic acid (TFA) over 20 minutes.

5.3 Results

High Resolution Mass Spectrometry

High resolution mass spectrometry was performed on dopamine (Figure 18**Error! Reference source not found.**) and trideuterated dopamine (Figure 19Figure 19**Error! Reference source not found.**). A comparison of the two mass spectra shows that the substitution is complete. By ^{1}H-NMR, the protons in the methylene groups (2.8 and 3.1 ppm) were still present but the aromatic protons between 6.6 and 6.8 ppm were not detectable (Figure 20**Error! Reference source not found.**). From ^{1}H-NMR, the substitution was estimated to be ≥98%.

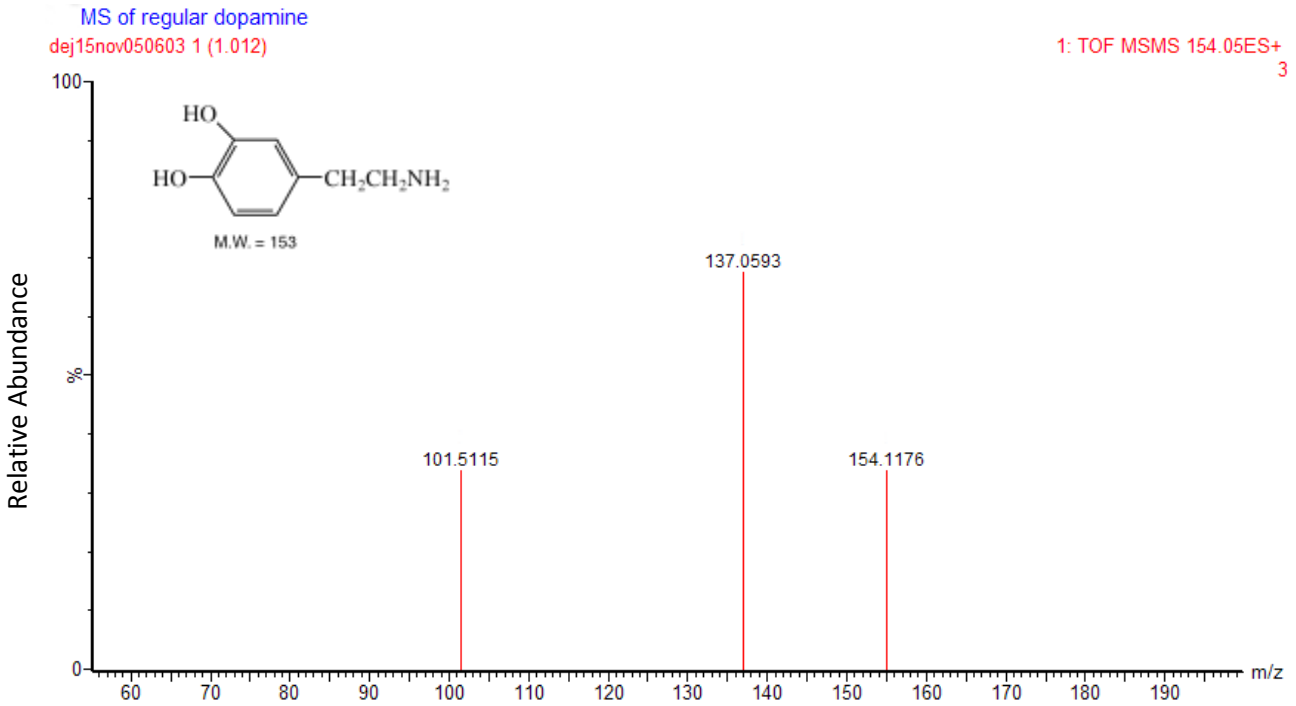

Figure 18. High resolution mass spectrometry analysis of dopamine. Dopamine is identified as m/z =154.1 showing fragments m/z=101.5 and 137.1.

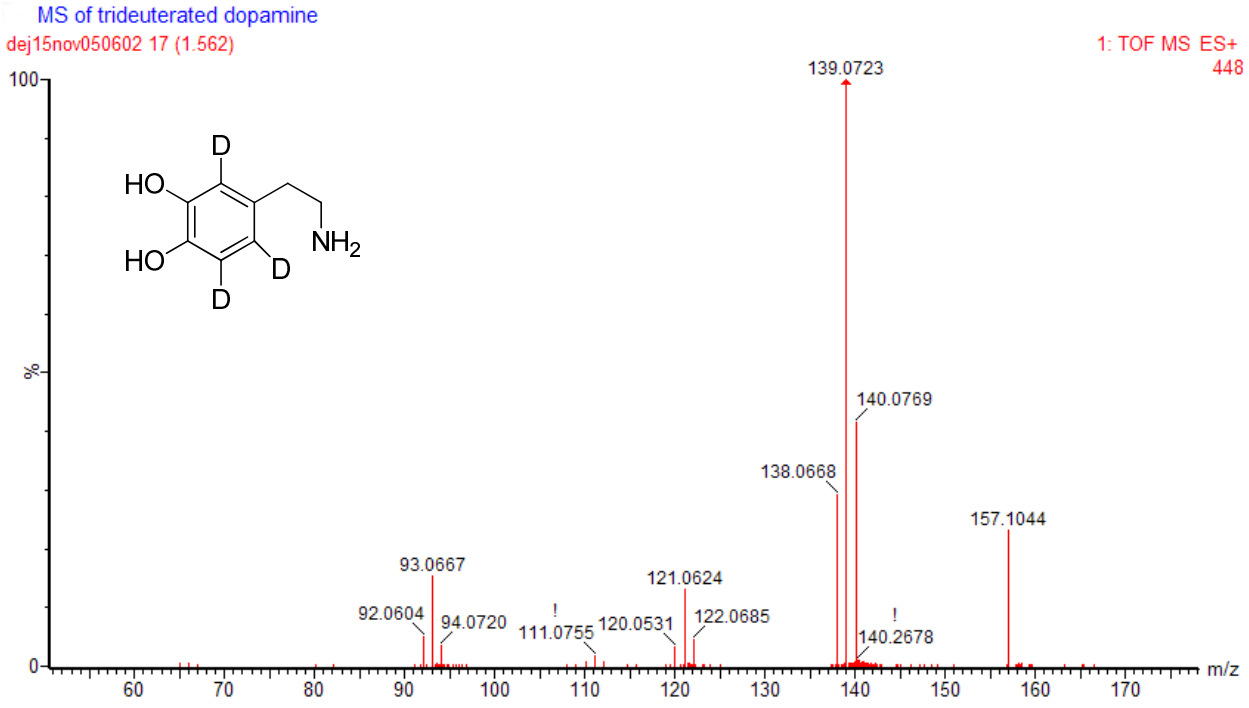

Figure 19. High resolution mass spectrometry analysis of trideuterated dopamine. Trideuterated dopamine is identified as m/z=157.1 showing fragments m/z= 139.1 , 121.1, and 93.1.

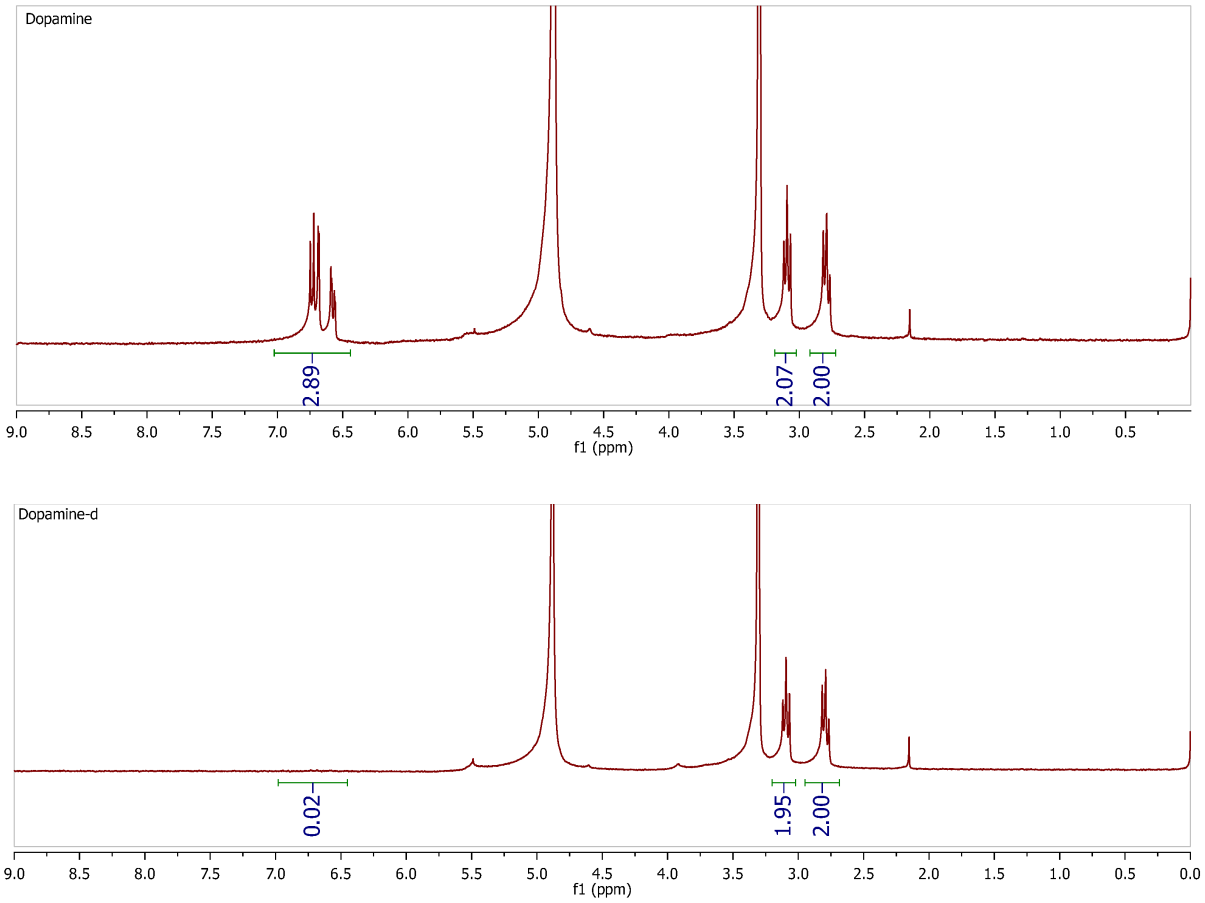

Figure 20. ^{1}H NMR traces of dopamine and deuterated dopamine in methanol-d_4. The peak at 3.31 ppm is the residual solvent peak, 4.87 ppm is water.

General Catalysis in Maleic Acid

The trends for buffer catalysis in phosphate buffer were much stronger than those for maleate buffer. The observed trend at constant buffer concentrations of 20 mM suggest a linear trend, however at 40 mM and 80 mM, there are too many inconsistencies to suggest a trend (Figure 21). These data series were repeated; however this did not help in determining which data point is the outlier. More data points are necessary to determine if there is a linear dependence on concentration of maleic acid and uncover a possible error in the data series.

The rate constants did not increase as the concentration of maleic acid buffer increased at a pH of 5.7; rather, it seems as if there is an exponential or parabolic trend. If there was a linear trend, this would indicate general buffer catalysis. This series was repeated several times, giving the same results. This is most likely due to an experimental error that has not been discovered yet. The experiments need to be repeated until acceptable results are obtained.

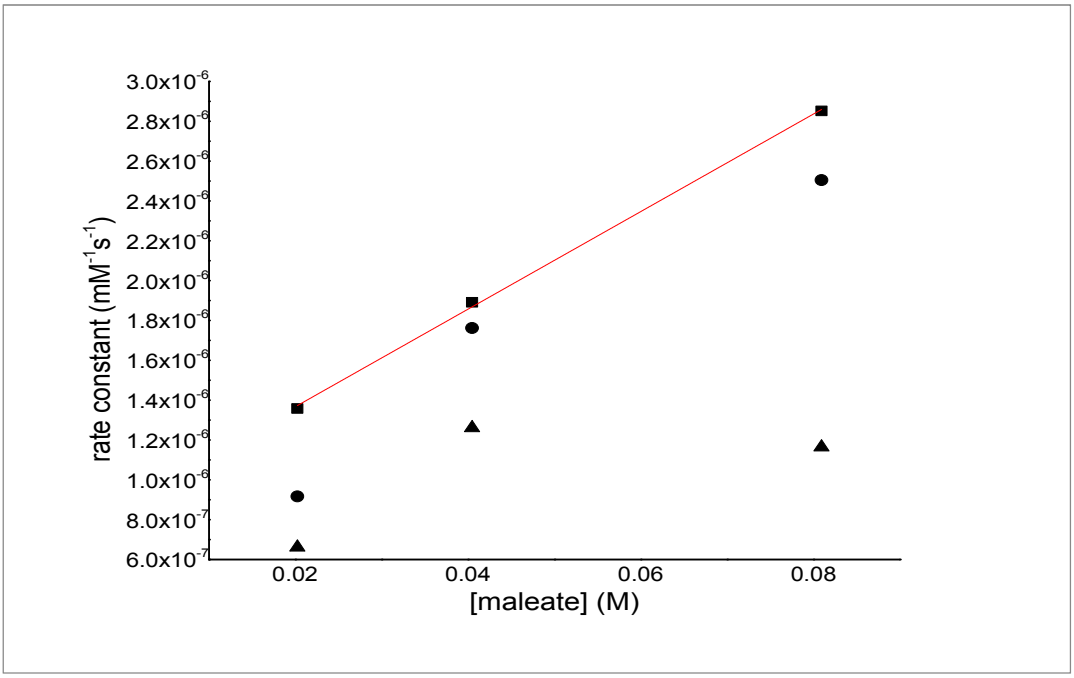

Figure 21. Rate constant dependence on the concentration of maleate for the reaction of dopamine at a constant concentration with pH increasing, producing THI. (▲)pH 5.7 (●) pH 6.1 (■)pH 6.60 linear regression results give a relationship of k_{obs} *= 2.503 ± 0.08 x* 10^{-7} $mM^{-1}s^{-1}M$ *x + 8.53 ± 0.20 x* 10^{-7} $mM^{-1}s^{-1}$.

Curtin-Hammett Principle Application

In phosphate buffer, the ratio of products THI/isoTHI, show a dependence on the concentration of total buffer (Figure 11). The data for maleate buffer does not conclusively demonstrate this. The data points should converge, which would indicate a trend and allow for the determination of the acid/base catalysis rate constants. The maleic acid data set (Figure 21) has discrepancies. More concentrations will need to be evaluated to determine an accurate trend for maleate buffer.

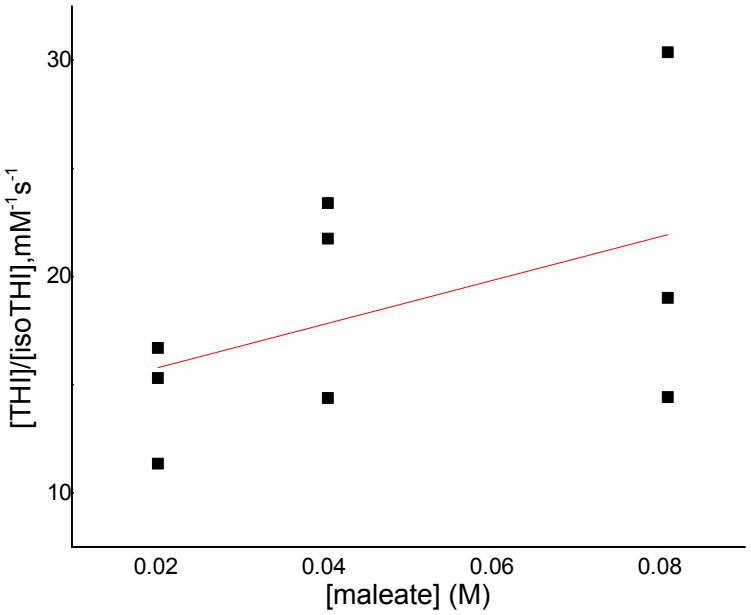

Figure 22. Ratio of THI product over isoTHI product dependence the concentration of total maleate buffer. The linear regression results give y=24 ± 4 $mM^{-1}s^{-1}M^{-1}$ x + 7. ± 3 $mM^{-1}s^{-1}$.

Kinetic Isotope Effects

To study kinetic isotope effects, [2,5,6-^{2}H]-dopamine (or simply "deuterated dopamine" from this point forward) was prepared by reacting commercial dopamine with D_2O under high temperature and pressure.

For small kinetic isotope effects, it is necessary to correct observed kinetic isotope effect date for low ^{2}H incorporation by the following equation where *x* is the fraction deuterated or $A_o^*/(A_o + A_o^*)$ where A^* refers to deuterated dopamine.[31]

$$KIE_{corrected} = x/(KIE_{observed} - 1 + x) \quad \text{Eq. 24}$$

Because of the large magnitude of all kinetic isotope effects observed in this work, the reported KIE values are uncorrected for low, incomplete incorporation of ^{2}H in the deuterated dopamine. Such corrections would be smaller than the uncertainty in the rate constant measurements.

In separate reactions conducted at the same time, deuterated dopamine reacted at a slower rate than the natural abundance dopamine in both phosphate and maleic acid buffer (

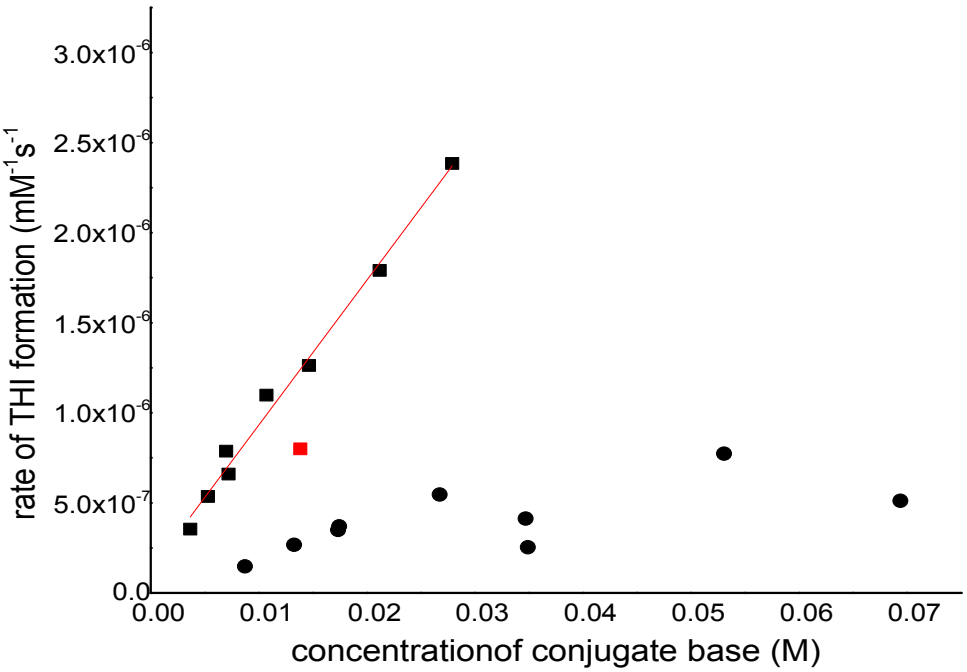

Figure 23Figure 24). Because the deuterated dopamine rates are slower than the natural abundance species, this demonstrations that the removal of the deuterium/hydrogen occurs in the limiting transition state for this multi-step reaction.

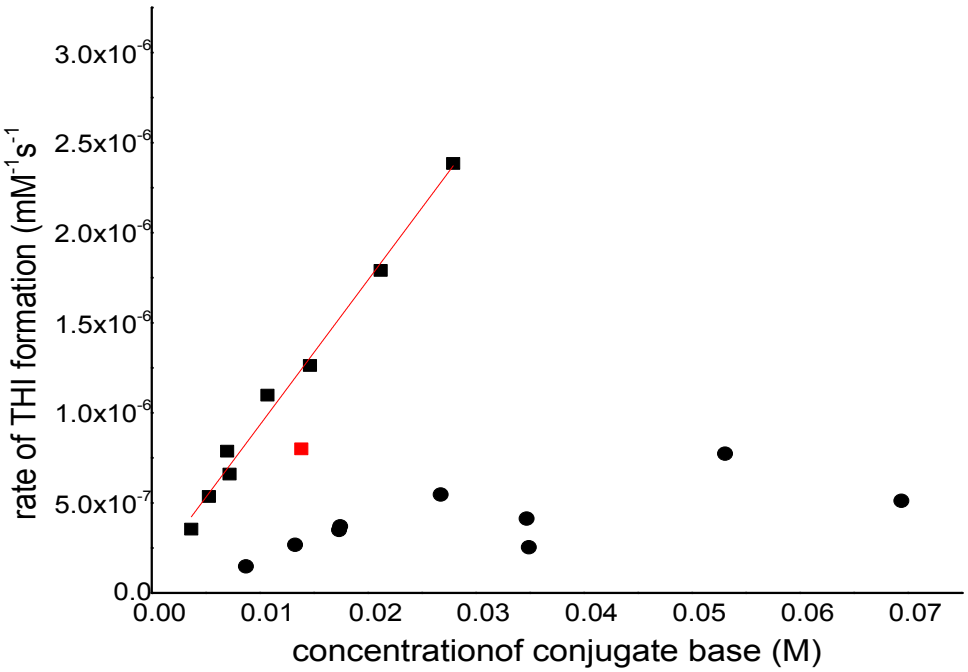

Figure 23. Observed rate of THI formation dependence on the concentration of conjugate base of phosphate (■) and maleic acid (●) buffers for the reaction of deuterated dopamine, producing THI. Line of best fit is y=8.5 ± 0.4 x10^{-5} mM^{-1}s^{-1}M^{-1} x + 5 ± 3 x 10^{-8} M with R^2= 0.99 for the reaction in phosphate buffer. The 40 mM phosphate pH 6.89 data point was excluded from this analysis under the assumption that it is an outlier due to experimental error.

For each condition, the observed second order rate constant is three to sevenfold slower for deuterated dopamine, indicative of a primary isotope effect (Figure 24). The range for primary KIE's is 5-8.[30] These results suggest that the final step of base catalyzed deprotonation (step 6 in Scheme 7) is rate limiting for this Pictet-Spengler reaction in both buffers.

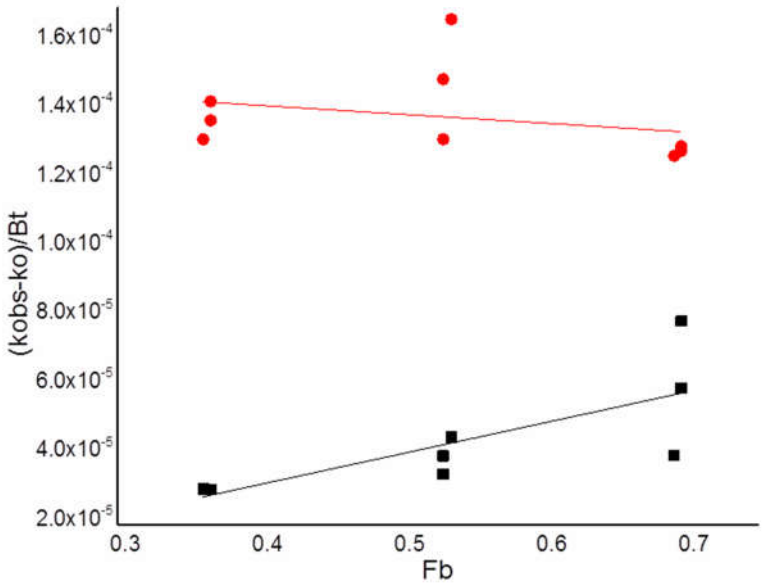

Figure 24. Comparison of the dependence of $\frac{k_{obs}-k_o}{B_t}$ on fractional base of the deuterated reaction (■) and natural abundance reaction(●) in phosphate buffer.

As noted in the previous chapter, this reaction is first order in base concentration. When the observed second order rate constants for THI formation are plotted against acid concentration for each condition, no trend is observed (Figure 12). The rate of THI product formation from deuterated dopamine is also first order in base concentration, however, the correlation is not as strong in maleic acid buffer (Figure 23). Given that these reactions were slower, the peak integrations relied on smaller values that may have introduced error. Furthermore, the instability of the reactants and products in solution also may have contributed to error in the measurement of these slower reactions. Likewise, the correlation is not as strong for isoTHI (Figure 25). This is most likely due to the small peak size of isoTHI in comparison to the other peaks, which increases the error.

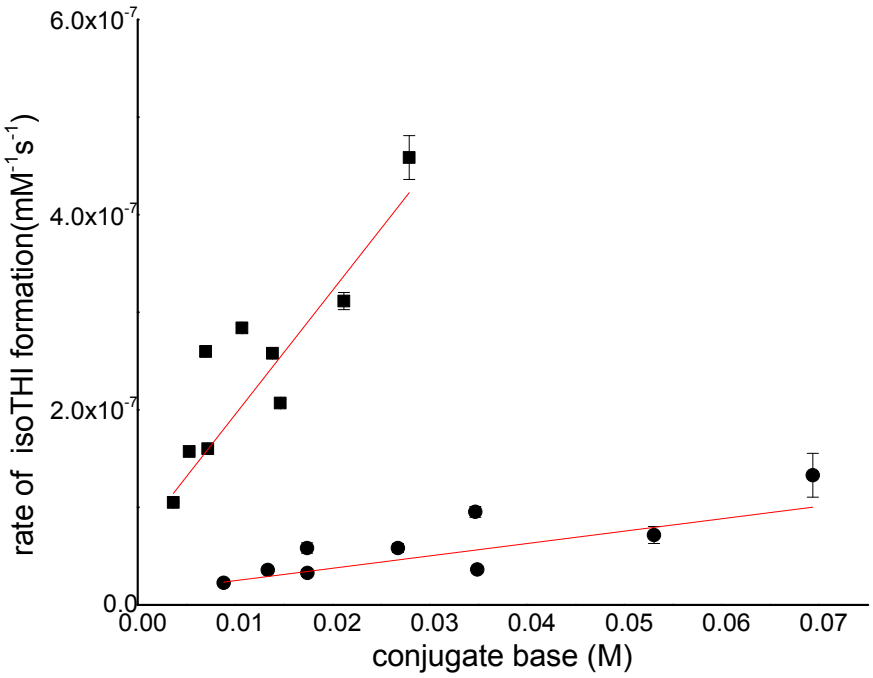

Figure 25. Observed rate of isoTHI formation dependence on the concentration of conjugate base species of phosphate buffer (■) and maleic acid buffer(●) of the reaction with deuterated dopamine, producing the isoTHI species. Line of best fit is $y=(1.3 \pm 0.3)\times10^{-5} mM^{-1}s^{-1}M^{-1} x + (7 \pm 2)\times10^{-8} M$ *with* $R^2= 0.86$ *for the reaction in phosphate buffer and* $y=(1.3 \pm 0.4)\times10^{-6} mM^{-1}s^{-1}M^{-1} x + (1.2 \pm 0.7)\times10^{-8} M$ *with* $R^2= 0.76$ *for the reaction in maleic acid buffer.*

The observed KIEs do not follow a discernable trend and exhibit significant variation. The origin of this variation is unclear. It may be due to experimental error. These experiments will need to be replicated with freshly prepared solutions and more concentrations measured to uncover trends in the KIE values.

Despite the variability in the KIE data, it is clear that our data shows a significantly large primary KIE. The average KIEs are around 5 and 4 in phosphate and maleate buffers, respectively. The following possibilities could explain the large KIE: either steps 5 and 6 have the same transition state (Figure 28) or the reverse reaction for step 5 is fast (Figure 27). If there was no kinetic isotope effect, the reaction coordinate for steps 5 and 6 for the Pictet-Spengler reaction would depict the energy profile in Figure 26.

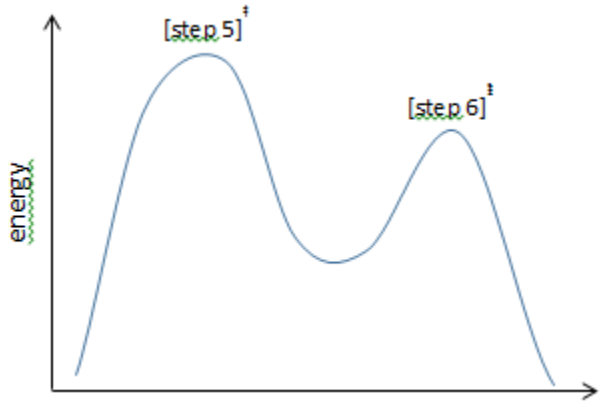

Figure 26. Reaction coordinate diagram for no kinetic isotope effect.

Figure 27 portrays the reaction coordinate for a small kinetic isotope effect (1-3) where step 5 is fast; however, this is not represented in our data. The other possibility is shown in the reaction coordinate

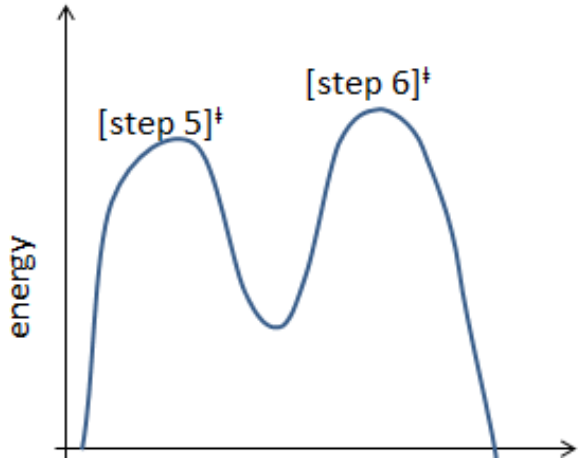

Figure 27. Reaction coordinate diagram for a small kinetic isotope effect.

for a large KIE (>3), (Figure 28). Steps 5 and 6 have the same transition state therefore, the rate for a large KIE (>3), (Figure 28). Where steps 5 and 6 have the same transition state therefore, the rate equation would be equal to [phosphate]^2. Because the base concentration increases linearly with rate, it is clear that either step 4 or 5 in Scheme 7 is the rate-limiting step. The observation of a large primary KIE strongly supports that the final deprotonation of the aromatic ring (step 5) as being rate limiting. We see that the KIE is not apparently dependent on the amount of buffer, (Figure 10). The large magnitude of the KIE is quite unusual for an electrophilic aromatic substitution reaction. Step 4 in Scheme 7 ring formation, is not typically expected to be a fast step because this reaction breaks aromaticity and reduces entropy. However, the 3-hydroxyl group clearly activates the ring and reduces this barrier. A computational study of the relative energy of these reaction barriers is in progress. Initial results suggest that phosphate may uniquely combine steps 5 and 6 into one step with one transition state (Figure 25). The current data are qualitatively consistent with this model and rule-out rate limiting ring closure (Figure 23). The current data are not clean enough to determine if there is a change in the kinetic isotope effect with maleic acid or if maleic acid functions by a different mechanism.

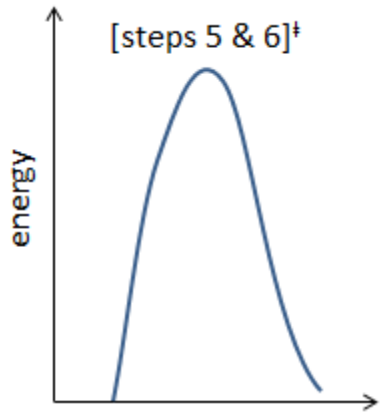

Figure 28. Reaction coordinate for a large kinetic isotope effect.

Kinetic Isotope Effects in Other Studies

The final deprotonation step has been found to be limiting for indole Pictet-Spengler reactions of tryptamine with propanal.[29] In that study, the observed effect was 2.7, a relatively small in magnitude for a primary KIE. Just as this dopamine Pictet-Spengler reaction is linearly dependent on base catalyst, the tryptamine reaction was linearly dependent on the concentration of acid catalyst. Thus, acid-catalyzed steps were significantly rate limiting in the tryptamine reaction. In general, the expression of the primary KIE for the isotopically dependent rate limiting step can be attenuated by other steps that are significantly rate limiting.[32] In the case of the tryptamine Pictet-Spengler reaction, this effect was verified by a strong linear dependence of the KIE on the concentration of acid catalyst. It was concluded that the mechanism was similar for both conditions. Therefore, the presence of an acid-catalyzed rate-limiting step most likely reduced the apparent value of the base-catalyzed isotopically dependent deprotonation. In contrast, the dopamine Pictet-Spengler reaction is base dependent, the KIE is close to the expected theoretical maximum for a primary KIE, and does not apparently vary with base or acid concentration (though this needs to be confirmed with higher quality data). Together, these observations suggest that the final deprotonation step is the only significant rate limiting step in the dopamine reaction with aldehyde. Acid catalyzed steps do not interfere with our ability to measure the KIE.

In the study of the tryptamine Pictet-Spengler reaction, the 2.7 magnitude of the KIE was similar in both enzymatic and acetic acid buffer reactions. Luk et al. studied the enzymatic mechanism of this Pictet-Spengler reaction norcoclaurine synthase (NCS) and observed a KIE of 1.7 for $(V_{max}/K_m)_H/(V_{max}/K_m)_D$. This study used dopamine and deuterated dopamine prepared by the same procedure. However, instead of propanal, the enzyme reaction was carried-out with 4-hydroxy-phenylacetaldehyde. This study did not examine isotope effects on the equivalent non-enzymatic reaction. Our finding that the KIE for the non-enzymatic reaction of dopamine is significantly higher suggests that steps other than deprotonation are significantly rate limiting in NCS, and therefore reduce the magnitude of the kinetic isotope effect in the phosphate buffer-catalyzed reaction system. It should be noted that the kinetic isotope effect measured for the enzymatic reaction followed the competition of deuterated and natural abundance dopamine

within the same reaction.[33] Observation of relative rate constants based on the ratios of the product distribution is a powerful method because it measures KIEs with higher precision. However, KIEs measured by such a method must be interpreted differently than KIEs measured from direct comparison of two separate reactions.[34] In such experiments, steps that have no analog in the buffer-catalyzed reaction, such as substrate binding and release of product measurements may be significantly rate limiting. Therefore, unless additional experiments are performed to verify an enzyme primary kinetic isotope effect is the intrinsic effect for the reaction, it cannot be compared to a chemical KIE because of other rate limiting steps that are introduced by enzyme reactions.[35] The intrinsic isotope effect for the enzymatic reaction would need to be measured for both $(V_{max}/K_m)_H/(V_{max}/K_m)_D$ and $(V_{max})_H/(V_{max})_D$ by measuring the these enzymatic kinetic constants in parallel reactions instead of by isotope competition in the same reaction.

In electrophilic aromatic substitution, a small, inverse secondary KIE is typically observed. Such an effect indicates that the isotopic bond substitution bond is not being broken and that the reaction for the deuterated reactant proceeds faster. [30] This effect is commonly observed because the slowest step is typically the attack on the ring. In general, this step is usually rate limiting as well[36], depending on the rate limiting step. This suggests that the KIE is secondary and another step is rate limiting.

Most electrophilic aromatic substitutions studied do not have a primary isotope effects because k_1 is large and k_2 and k_{-1} are small (Figure 29).[36] The slowest step is not actually rate limiting because the faster second step is actually the highest energy barrier.

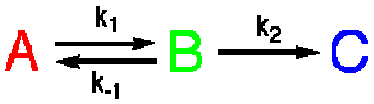

Figure 29. First step reversible reaction where k_1 is the formation of isoTHI , k_2 is the formation of THI and k_{-1} is the starting material, dopamine.

Pesnot proposed two pathways for the Pictet-Spengler reaction where phosphate acts as a base after the formation of iminium intermediate (Scheme 4). Phosphate, anion or dianion, undergoes nucleophilic attack on the iminium intermediate, thereby forming a highly reactive aminophosphate that is in equilibrium with the iminium. In his proposed path a, phosphate acts as a base to deprotonate and activate cyclization. Phosphate then mediates intramolecular rearomatization. In Pesnot's path b, phosphate mediates intramolecularly rearomatization. The favored pathway for this reaction is the formation of a carbinolamine, which then facilitates catalysis, allowing for rearomatization. However, this was not supported by our data. We find the reaction to be base catalyzed, but no intermediate due to rearomatization and cyclization occurring simultaneously.

Additionally, there is no evidence that shows that the aminophosphate adduct exists in this reaction. Interestingly, Pesnot's hypothesized mechanisms both require two phosphate ions up to and including the final deprotonation step. If rearomatization were rate limiting in such a model, as our data shows, then the rate dependence would be:

$$rate = [phosphate]^2$$

Although the current data has considerable scatter, they do not suggest such a rate dependence on phosphate. We hypothesize that our very large primary KIE is due to cyclization and rearomatization occurring simultaneously with no intermediate (Scheme 4) and that a second equivalent of phosphate is not required to deprotonate the phenol. In addition to our data, Dr. Ruben Parra has modeled this reaction and found that a single transition state for both Steps 5 and 6 is the lowest energy pathway. This provides an explanation for the large KIE values as there are no preceding steps which would decrease the KIE. Based on this data, we are able to conclude that final step, step 6, is the rate limiting step and that one equivalent phosphate buffer is responsible for catalysis.

The effects of acid and base appear to cancel each other out in terms of regioselectivity of the reaction for THI versus isoTHI. The total phosphate concentration, not the concentration of an individual species, is linearly correlated to the THI/isoTHI ratio. Because two conformations (Figure 11) of the same iminium intermediate give rise to the two different products, THI and isoTHI, the Curtin-Hammett principle applies such that the ratio of the two kinetic products is proportional to $\Delta\Delta G^{\ddagger}$ for the rate limiting step of the two reactions when the reaction is carried-out under kinetically selective conditions.[26] The large primary KIE observed for all reactions suggests that the final deprotonation is the rate limiting step in all reaction conditions studied. Within the limits of the current dataset, the reaction appears to be linearly dependent on buffer concentration. This indicates that there is one equivalent of buffer in the rate limiting transition state.[37] Combining these two pieces of information, the transition state structures in Scheme 9 are drawn to indicate the final deprotonation step without simultaneous protonation of the ring.

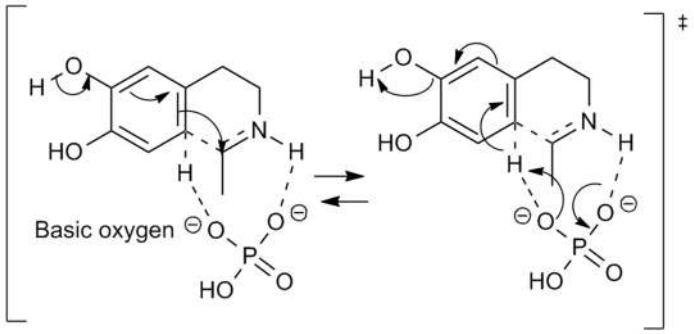

Scheme 9. Proposed reaction of phosphate where a one-step deprotonation and cyclization with no intermediate occur. Phenol deprotonation is not required.

Chapter 6 – Conclusions and Future Work

The mechanism of the Pictet-Spengler reaction of dopamine with propanal in maleic acid is apparently comparable to that in phosphate buffer. The rate of reaction clearly depends on the concentration of buffer. In addition, [HA] is not the rate-limiting catalytic species. Although there is a strong first order rate in the base concentration in both buffers, it is not as strong in maleic acid buffer. When observing the reaction mechanism, step 4 (rearomatization) is in a base dependent equilibrium and step 5 (electrophilic cyclization) is base catalyzed (Scheme 7). This confirms that the reaction is dependent on the base concentration. When determining which step is rate limiting, the deuterated dopamine reacted at a slower rate than the natural abundance species; in both buffers the rate was 3-fold to 4-fold slower. This suggested that step 6, deprotonation, is rate limiting. In addition, general base catalysis is observed, where k_b in phosphate buffer is about an order of magnitude faster than in maleate buffer, further confirming that the reaction is dependent on the base concentration.

In the midst of studying the reaction, and isomer of tetrahydroisoquinoline was seen, which we call isoTHI. Interestingly, no previous work has mentioned this product. Although we were not able to isolate and purify isoTHI for this work, our goal is to do this and to verify the extinction coefficients we calculated. The reaction in phosphate buffer showed that the reaction is dependent on buffer concentration and pH. Previous work found the Pictet-Spengler reaction of tryptamine with aldehydes to be acid catalyzed. We found no trend for acid catalysis in a rate limiting step, only base catalysis for both maleic and phosphate buffers. However, stronger trends are seen for phosphate buffer. Maleic acid buffer trends fall apart as the pH reaches the pKa of maleic acid. Further work on comparable buffers would be helpful to see if they would also follow this trend and if there is phosphate specificity seen.

A kinetic isotope effect is seen in both phosphate buffer and maleic acid buffer. It is quite large, in fact, indicating a primary isotope effect. This occurs because rearomatization and cyclization occur simultaneously. A currently unpublished computational study by Dr. Ruben Parra found a low energy pathway for the cyclization and rearomatization steps for the formation of a model compound analogous to THI. In this pathway, the final deprotonation step was rate limiting and dibasic phosphate (HPO_4^{2-}) was the best base catalyst. A schematic of the rate limiting transition states found are shown in Scheme 10. In these structures, phosphate may exhibit enhanced basicity due to the unique bridged structure or it could be that this bridged structure catalyzes both steps 5 and 6 as a single transition state. Unfortunately, we were unable to conclusively observe a different catalytic mechanism in maleic acid buffers. These slower reactions gave poorer results. This was most likely the result of interference from slow side reactions that decompose the reactants and products that become more significant when the reaction is slower, as was the case for reactions with deuterated dopamine and maleic acid buffer.

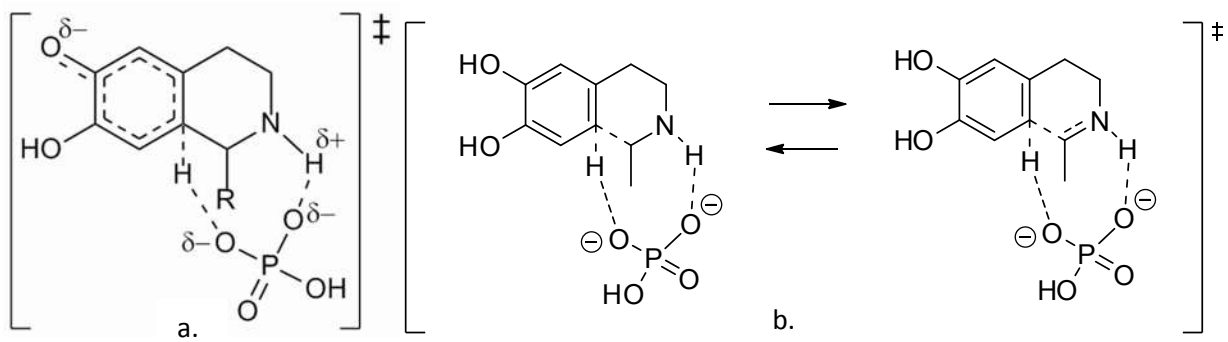

Scheme 10. Proposed rate limiting transition states of model compound analogous to THI.

Future Directions

Dopamine is an unstable catechol. Our inability to obtain trends in some cases made be due to the presence of oxidative decomposition of the catechol functional group in both dopamine and the Pictet-Spengler reaction products. The resulting quinones are not generally observed by HPLC because they rapidly polymerize to multiple species that elute late in our method or precipitate and are not injected. Elimination of the catechol group should improve the overall quality of the data. In order to isolate THI and isoTHI, the below reactions can be used to prepare an amine substrate that is less vulnerable to oxidation due to an absent catechol. This compound will then permit the study of Pictet-Spengler reactions for longer time frames. This will be helpful as I have evidence that the stock solution of deuterated dopamine decomposed a bit and may have contained some reactive side products.

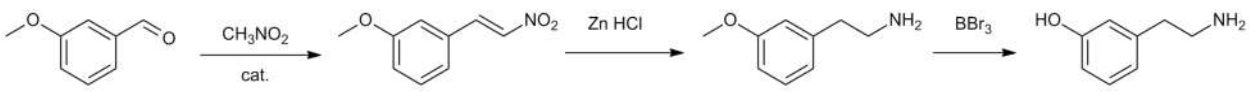

Scheme 11. Proposed preparation amine substrate with higher stability.

Additionally, the boiling point of propanal is 46 °C. It is possible that the concentration of aldehyde is drifting while our kinetics experiments are running. This could significantly affect the apparent rate constant measured for slow reactions and may make them difficult to compare to faster reactions, thus impacting the trends for kinetic isotope effect measurements. Propanal was selected because its high water solubility made it suitable for pseudo first order kinetics. However, a less volatile aldehyde may improve the trends in future experiments.

Finally, internal competition experiments provide high quality KIEs. It is possible that an isotopically sensitive method like NMR could be used to measure KIEs by this alternative method.

References

1. Roberts, M. F., *Alkaloids: Biochemistry, Ecology, and Medicinal Applications*. 1998.
2. Buckingham, J., *Dictionary of Alkaloids*. 1st edition ed.; CRC Press: 2010.
3. (a) Hagel, J. M.; Facchini, P. J., Benzylisoquinoline Alkaloid Metabolism: A Century of Discovery and a Brave New World. *Plant and Cell Physiology* **2013,** *54* (5), 647-672; (b) The Genome of Physcomitrella patens ssp patens ecotype Gransden 2004. http://genome.jgi-psf.org/Phypa1_1/; (c) Pesnot, T.; Gershater, M. C.; Ward, J. M.; Hailes, H. C., Phosphate mediated biomimetic synthesis of tetrahydroisoquinoline alkaloids. *Chem. Commun.* **2011,** *47* (11), 3242-4.
4. Liscombe, D. K. Discovery of Novel Alkaloid Biosynthetic Genes Using Biochemical Genomics. University of Calgary, 2008.
5. Cox, E. D.; Cook, J. M., The Pictet-Spengler condensation: A new direction for an old reaction. *Chem. Rev.* **1995,** *95*, 1797-1842.
6. (a) Stöckigt, J.; Antonchick, A. P.; Wu, F.; Waldmann, H., The Pictet–Spengler Reaction in Nature and in Organic Chemistry. *Angewandte Chemie International Edition* **2011,** *50* (37), 8538-8564; (b) Pictet, A. a. S., Theod., Über die Bildung von Isochinolin-derivaten durch Einwirkung von Methylal auf Phenyl-äthylamin, Phenyl-alanin und Tyrosin. *Berichte der deutschen chemischen Gesellschaft* **1911,** *44* (3), 2030-2036.
7. Yokoyama, A.; Ohwada, T.; Shudo, K., Prototype Pictet−Spengler Reactions Catalyzed by Superacids. Involvement of Dicationic Superelectrophiles. *The Journal of Organic Chemistry* **1998,** *64* (2), 611-617.
8. Benjamin R. Lichman, M. C. G., Eleanor D. Lamming,Thomas Pesnot,Altin Sula, Nicholas H. Keep, Helen C. Hailes,John M. Ward, Dopamine-first' mechanism enables the rational engineering of the norcoclaurine synthase aldehyde activity profile. *FEBS Journal* **2015,** *1137-1151*.
9. Parra, R. M., Justin, Structural and Energetics Aspects of a Proposed Mechanism for the Phosphate-Mediated Pictet-Spengler Cyclization Reaction: A Computational Study. *Computational and Theoretical Chemistry* **2015**.
10. Crowe, S. Synthesis and Evaluation of Unnatural HPAA, Nocroclaurine, and Tyramine Analogs. DePaul University, Chicago, IL, 2013.
11. Good, N. E.; Winget, G. D.; Winter, W.; Connolly, T. N.; Izawa, S.; Singh, R. M. M., Hydrogen Ion Buffers for Biological Research. *Biochemistry* **1966,** *5* (2), 467-477.
12. Perelygin, Y. P.; Chistyakov, D. Y., Boric acid. *Russian Journal of Applied Chemistry* **2006,** *79* (12), 2041-2042.
13. Alan S. Tracey, G. R. W., Esther S, *Vanadium: Chemistry, Biochemistry, Pharmacology and Practical Applications*. CRC Preess: 2007.
14. Lide, D. R., *CRC handbook of chemistry and physics : a ready-reference book of chemical and physical data*. CRC Press: Boca Raton, FL, 1994.
15. Potassium Phosphate Monobasic.
16. Mathews, C. K., K. E. Van Holde, Ean R. Appling, and Spencer J. Anthony-Cahill, *Biochemisty*. Benjamin/Cummings Pub: Redwood City, CA, 1990.
17. Salaun, F., Influence of mineral environment on the buffering capacity of casein micelles. *Milchwissenschaft 62* (1).
18. M, S., *Chemistry: The Molecular Nature of Matter and Change* 5th ed.; McGraw-Hill Higher Education: New York, 2008.
19. Herve, G., *Allosteric Enzymes*. CRC Press: 1989.

20. McElroy, W. D.; Glass, B., *Phosphorus Metabolism, Vol. I*. Johns Hopkins University Press: Baltimore, 1951.
21. (a) Rodolfo Quevedo, C. P., and Sonia Moreno, Heterogeneous Catalysts in Pictet-Spengler-Type Reactions. *Journal of Chemistry* **2012,** *2013*; (b) Rodolfo Quevedo, Edwin Baquero, Mario Rodriguez, Regioselectivity in isoquinoline alkaloid synthesis
Tetrahedron Letters **2010,** *51* (13), 1774-1778.
22. Maresh, J. J., Crowe, Sean O., Ralko, Arthur A., Aparece, Mark D., Murphy, Casey M., Krzeszowiec, Mark, Mullowney, Michael W. , Facile one-pot synthesis of tetrahydroisoquinolines from amino acids via hypochlorite-mediated decarboxylation and Pictet-Spengler condensation. *Tetrahedron Letters* **2014,** *55*, 5047-5051.
23. Philip R. Bevington, D. K. R., Data Reduction and Error Analysis for the Physical Sciences. **2003**.
24. Maresh, J. J.; Giddings, L.-A.; Friedrich, A.; Loris, E. A.; Panjikar, S.; Trout, B. L.; Stöckigt, J.; Peters, B.; O'Connor, S. E., Strictosidine Synthase: Mechanism of a Pictet−Spengler Catalyzing Enzyme†. *Journal of the American Chemical Society* **2007,** *130* (2), 710-723.
25. Jencks, W. P., *Catalysis in Chemistry and Enzymology*. McGraw-Hill: New York, 1969; p pp. 490-496.
26. Seeman, Effect of Conformational Change on Reactivity in Organic Chemisity. Evaluations, Applications, and Extenstions of Curtin-Hammet/Winstein-Holness Kinetics. *Chemical Reviews* **1983,** *83* (2), 83-133.
27. Ellis, K. J.; Morrison, J. F., Buffers of Constant Ionic Strength for Studying pH-Dependent Processes. *Methods in Enzymology* **1982,** *87*, 405-426.
28. (a) Mendes, P., Gepasi - a Software Package for Modeling the Dynamics, Steady-States and Control of Biochemical and Other Systems. *Computer Applications in the Biosciences* **1993,** *9* (5), 563-571; (b) Mendes, P., Biochemistry by numbers: simulation of biochemical pathways with Gepasi 3. *Trends in Biochemical Sciences* **1997,** *22* (9), 361-363; (c) Mendes, P.; Kell, D. B., Non-linear optimization of biochemical pathways: applications to metabolic engineering and parameter estimation. *Bioinformatics* **1998,** *14* (10), 869-883.
29. Maresh, J.; Giddings, L.-A.; O'Connor, S. E.; Friedrich, A.; Loris, E. A.; Panjikar, S.; Trout, B.; Stöckigt, J.; Peters, B.; O'Connor, S. E., Strictosidine Synthase: Mechanism of a Pictet-Spengler Catalyzing Enzyme. *J. Amer. Chem. Soc.* **2007,** *accepted on October 17, 2007.*
30. Carroll, F. A., *Perspectives on Structure and Mechanism in Organic Chemistry*. 2 ed.; Wiley: 2011.
31. F. W. Dahlquist, T. R.-M., Michael A. Raftery, Application of secondary .alpha.-deuterium kinetic isotope effects to studies of enzyme catalysis. Glycoside hydrolysis by lysozyme and .beta.-glucosidase. *Biochemistry* **1969,** *8* (10), 4214-4221.
32. Thompson, W. H., Kiefer, P. M. and Hynes, J. T, *ransition State Theory and Reaction Dynamics – An Overview, in Femtochemistry: With the Noble Lecture of A. Zwail (eds F. C. De Schryver, S. De Feyter and G. Schweitzer)*. Wiley-VCH Verlag GmbH: Weinheim, 2001.
33. Luk, L. Y.; Bunn, S.; Liscombe, D. K.; Facchini, P. J.; Tanner, M. E., Mechanistic studies on norcoclaurine synthase of benzylisoquinoline alkaloid biosynthesis: an enzymatic Pictet-Spengler reaction. *Biochemistry* **2007,** *46* (35), 10153-61.
34. Dr. Eric M. Simmons; Hartwig, P. J. F., On the Interpretation of Deuterium Kinetic Isotope Effects in C[BOND]H Bond Functionalizations by Transition-Metal Complexes. *Angewandte Chemie International Edition* **5 March 2012,** *51* (13), 3066-3072.
35. Cleland, W. W., The Use of Isotope Effects to Determine Transition-State Structure for Enzymic Reactions. *Methods in Enzymology* **1982,** *87*, 625-641.
36. Zollinger, H., Hydrogen isotope effects in aromatic substitution reactions. *Advan. Phys. Org. Chem. (V. Gold, editor, Academic)* **1964,** *2*, 163-200.

37. Jackson, A. H.; Smith, A. E., Electrophilic substitution in indoles. II. Formation of 3,3-spirocyclic indole derivatives from tryptamines and their rearrangement to b-carbolines. *Tetrahedron* **1968,** *24* (1), 403-13.